ESTIMATION OF EFFECTIVE ELASTIC THICKNESS IN REGIONS OF REDUCED TOPOGRAPHY: A CASE STUDY IN THE PERMIAN BASIN

A Thesis

by

SAMUEL MARTIN PRICE

Submitted to the Office of Graduate and Professional Studies of
Texas A&M University
in partial fulfillment of the requirements for the degree of

MASTER OF SCIENCE

Chair of Committee,	Mark Everett
Committee Members,	Nicholas D. Perez
	Michael King
Head of Department,	Mike Pope

December 2018

Major Subject: Geophysics

ABSTRACT

The effective elastic thickness (Te) of the lithosphere is a geometric measure of its flexural rigidity and is determined by isostatic forces, crustal composition, thermal properties, and deformation history. As such, Te can be used to constrain mechanical properties of the lithosphere and reflects the tectonic evolution of both continental and oceanic plates. Inverse spectral analysis techniques such as gravitational admittance and coherence utilize gravity and topography data in conjunction with various plate models to estimate Te across a region. 2-D gravitational coherence has been widely used in continental flexural studies, although recent work has revealed that coherence can significantly bias Te estimations in regions of reduced topography. The Delaware and Midland Basins of west Texas are such regions that have undergone significant but poorly quantified magnitudes of erosion, and application of spectral analysis to estimate Te has proved difficult. A revised method of estimating Te is herein provided that utilizes a modified form of the observed 1-D gravitational admittance. The method introduces a topographic regularization parameter (TRP) to account for the reduction of mid-to-high wavenumber spectral power associated with erosion and interpolation of unevenly spaced data. Implementation of the TRP increases the spectral power of the topography, effectively producing artificial, uncompensated low-to-mid wavelength topography which improves inversion results. A 2-D effective elastic thickness map is produced across the Permian Basin using the revised admittance calculation. Spatial resolution of Te estimates increased utilizing multi-trace 1-D admittance over 2-D coherence. The resulting regional variation in Te reported herein correlates with known geology and provides insight into the future development of Te estimation and geologic interpretation of structures in basins worldwide.

ACKNOWLEDGEMENTS

First and foremost, I would like to thank Mark Everett for his guidance in assisting me with this project. His support both as a faculty advisor and as a mentor cannot be understated. My success within the graduate program at Texas A&M University is largely a result of his generosity, and my development as a scientist is due mostly to the opportunities he presented me by accepting me as his student.

Nick Perez also contributed significantly to this project since its inception. I thank him sincerely for his assistance and mentorship.

I also would like to extend my gratitude to Mauro Becker and Andrea Miceli-Romero within the Chevron Center of Research Excellence Basin Modelling Program at Texas A&M University. Their consistent encouragement motivated me to keep working and deliver a great project.

The Department of Geology and Geophysics Department at Texas A&M University requires recognition for their integrated and open approach to research collaboration and mentorship. I count myself fortunate for the experiences and interactions I've had with world-renown scientists and scholars.

I would lastly like to thank my family for their unwavering support. Never have they questioned my ability to succeed.

CONTRIBUTORS AND FUNDING SOURCES

This work was supervised by Dr Mark Everett (Department of Geology and Geophysics) in conjunction with Dr Nicholas Perez (Department of Geology and Geophysics) and Dr Michael King (Department of Petroleum Engineering) of Texas A&M University.

Mark Everett and Nicholas Perez assisted the student with literature review and research focus. Data for this project is publicly available through the USGS and can be acquired online (Bankey 2006). Data processing and coding was performed by the student with assistance by Mark Everett. Interpretation of model results were made with aid of Nicholas Perez and Mark Everett. All other work was completed by the student independently.

Work for this study was funded by a two-year fellowship ($60,000) through the Chevron Center of Research Excellence (CoRE) Basin Modelling Program as part of the Berg-Hughes Center of Petroleum and Sedimentary Systems at Texas A&M University.

NOMENCLATURE

AGM	Abilene Gravity Minimum
CBP	Central Basin Platform
DB	Delaware Basin
LAB	Lithosphere-Asthenosphere Boundary
MOR	Mid-Ocean Ridge
MB	Midland Basin
NWS	Northwestern Shelf
OMTB	Ouachita-Marathon Thrust Belt
PB	Permian Basin
SGRP	Southern Granite-Rhyolite Province
TB	Tobosa Basin
Te	Effective Elastic Thickness
Ts	Seismogenic Layer Thickness
TRP	Topographic Regularization Parameter
VB	Val Verde Basin
YSE	Yield Stress Envelope

TABLE OF CONTENTS

Page

LIST OF FIGURES

LIST OF TABLES

LIST OF EQUATIONS

CHAPTER I

INTRODUCTION TO ISOSTASY AND FLEXURE

Flexural studies are based upon the concept of isostasy whereby the lithosphere, the outermost, rigid portion of Earth that includes the crust and upper mantle, tends toward gravitational equilibrium with the asthenosphere, the lower and more viscous portion of the mantle. The Lithosphere-Asthenosphere Boundary (LAB) separates the two layers at approximately the 1300°C isotherm and is marked by a contrast in the predominant form of deformation mechanics: the upper lithosphere deforms both elastically and through brittle failure while the asthenosphere accommodates strain mainly through plastic deformation. The mechanical and compositional structures of Earth are presented in Figure 1.1.

Figure 1.1 – Compositional and Mechanical Structures of the Earth

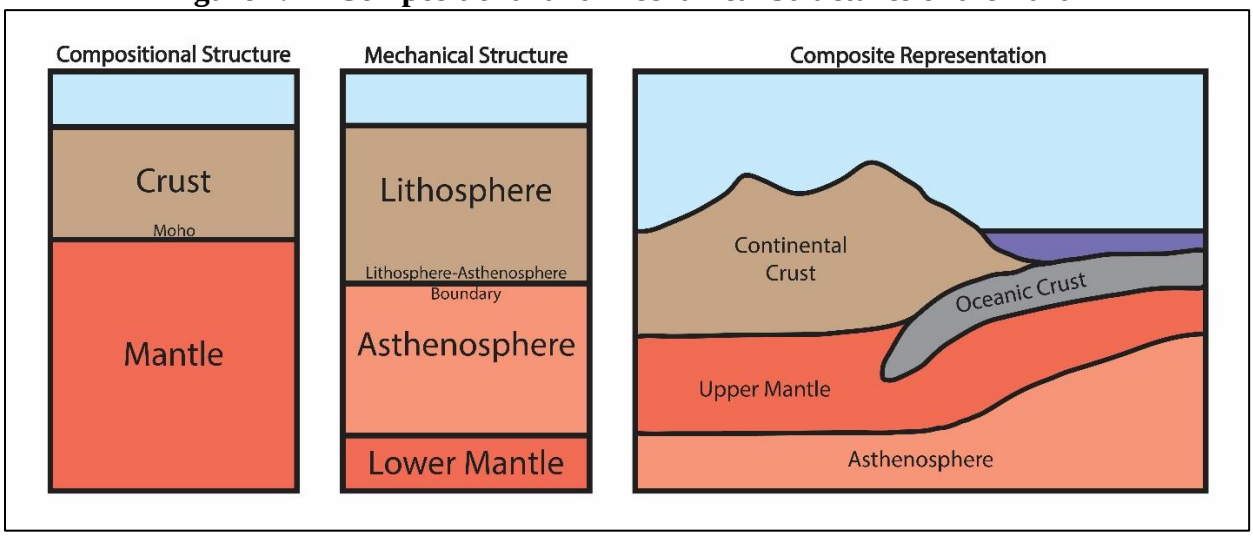

The compositional structure of the outermost portions of Earth is divided into the crust and mantle. The crust is dominated by silicate minerals and the mantle consists mostly of peridotite. The lithosphere includes the crust and uppermost mantle where brittle failure is the predominant deformation mechanism. Below the lithosphere resides the asthenosphere, a hot, viscous region which deforms plastically and flows like a fluid on geologic timescales.

Geologic processes such as orogenies, subduction, sedimentation, glaciation, and erosion redistribute mass within and across the Earth. The resulting mass density anomalies can be found both on Earth's surface and within the subsurface. Buoyancy forces acting within the asthenosphere continually re-establish isostatic equilibrium with the lithosphere through uplift and subsidence. The lithosphere is characterized by depth-integrated rigidity such that compensation for mass anomalies occurs regionally and produces a flexural profile that is based upon the depth and extent of the mass anomaly and the mechanical properties of both the lithosphere and asthenosphere.

Both continental and oceanic lithosphere are modified through flexure induced by mass loading and de-loading events. Figure 1.2 describes an ideal case of flexure whereby the progressive growth of seamounts adds mass onto oceanic crust, imposing vertical stresses and consequently flexing the lithosphere. However, the relative simplicity of this scenario is rarely observed within continental regions. The origin of continental and oceanic lithosphere, both in terms of their respective chemical composition and age, manifests in different flexural patterns which are largely controlled by their respective strength. Estimation of the effective elastic thickness (Te) is used to estimate the lithosphere's strength. The Te parameter represents the aggregate strength of the lithosphere if modelled as an elastic plate (Watts 2001). The value of Te is largely controlled by thermal properties, composition, tectonic stress orientation and magnitude, and plate age (Lowry and Smith 1995).

Figure 1.2 – Oceanic Flexure via Seamount Evolution

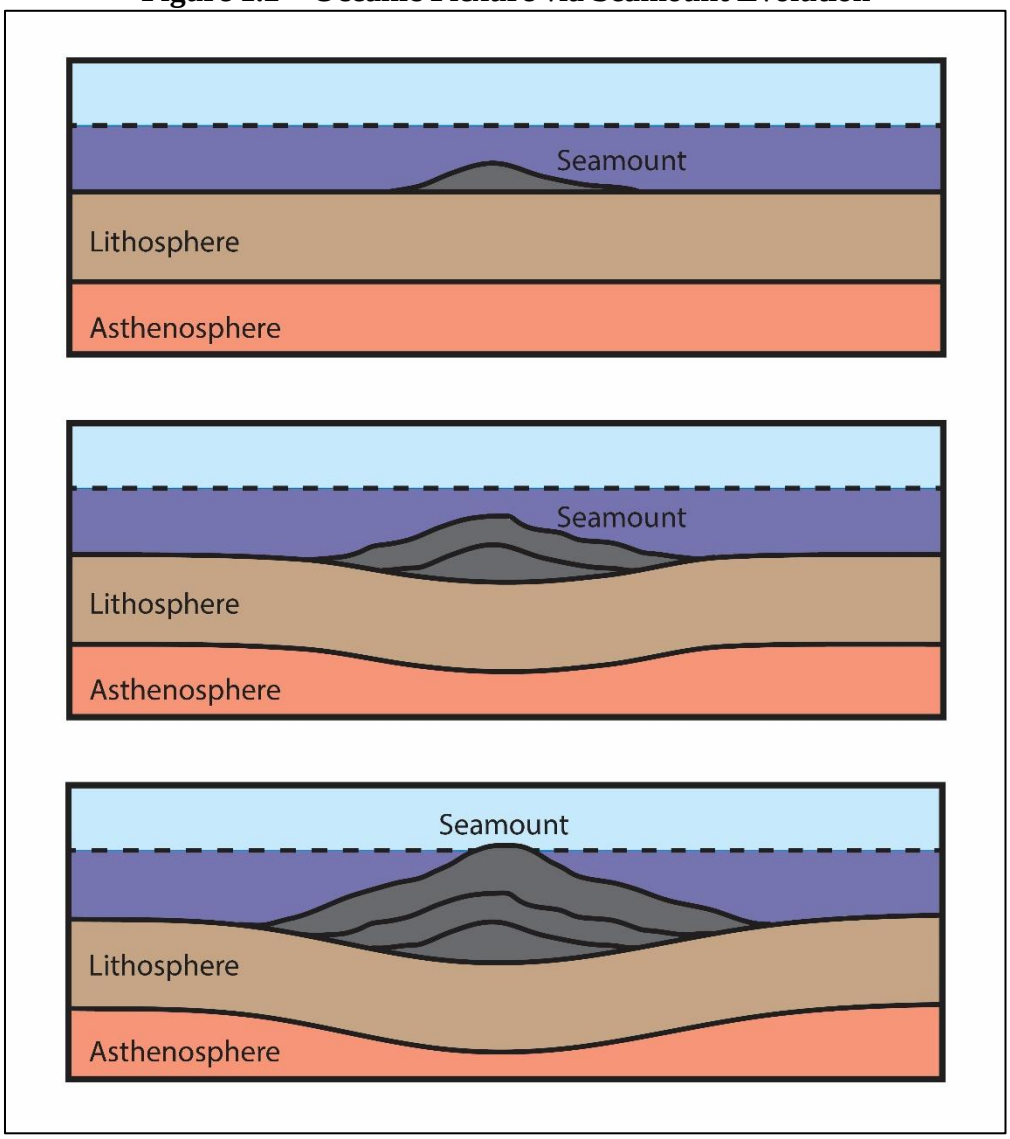

Representation of oceanic flexure induced by the progressive growth of seamount eruptions is pictured above. As additional mass is added onto the oceanic crust, the lithosphere begins to flex. The degree of flexure depends upon the magnitude of the load, the geometry of the load, and the strength of the lithosphere across the region.

Estimation of Te can be accomplished using gravity and topography data. A relationship between these two types of data can be formed in the spatial frequency domain, also called the wavenumber domain, to describe the interaction between mass loads and lithospheric flexure. Such a relationship may be understood conceptually by considering the material science equations that

relate vertical loading to the bending of an elastic or viscoelastic beam (Timoshenko and Woinowsky-Krieger 1959). By comparing the theoretical bending of an elastic beam with an observed flexural profile identified through analysis of gravity and topography data, an estimate of Te can be found using an inversion procedure. Two prominent techniques are available to estimate effective elastic thickness: gravitation admittance and gravitational coherence. Both techniques relate gravity and topography data to one another in the wavenumber domain. For reasons detailed in Section 3.5, only gravitational admittance will be utilized herein to estimate the effective elastic thickness of the North American plate across the Delaware and Midland Basins.

CHAPTER II

GEOLOGIC HISTORY OF THE PERMIAN BASIN

2.1 Permian Basin Overview

The Greater Permian Basin, more commonly referred to as the Permian Basin (PB), is located in western Texas and eastern New Mexico, spanning approximately 200,000 km^2 across 52 counties. The Permian Basin has a complex geologic history, and the region has undergone significant internal deformation through tectonic collision and rifting, resulting in its differentiation into numerous sub-basins separated by uplifted platforms. The largest two sub-basins, the Midland Basin (MB) and Delaware Basin (DB), are the foci of this study. The Central Basin Platform (CBP), a NW-SE trending uplifted basement block, separates the Midland and Delaware Basins. The Northwestern Shelf (NWS) bounds the CBP and DB to the north while the Val Verde Basin (VB) is situated to the south of CBP and MB. An interpretation of the present-day palestructures of the Permian Basin is presented in Figure 1.1.

The Permian Basin is the most prolific petroleum-producing basin in the United States. Extensive drilling of sedimentary sections has provided a wealth of information, allowing geoscientists to thoroughly characterize regional stratigraphy (e.g. Galley 1958, Adams 1965, Hills 1984, Wright 2011). Figure 2.2 displays an east-west oriented cross-section throughout the Permian Basin which shows the composition of sedimentary strata. Few wells in the Permian Basin have penetrated below the sedimentary layers and those that have mainly penetrated basement highs such as the CBP (Adams and Keller 1996). Knowledge of the basement elsewhere throughout the region has primarily been drawn from direct measurements of core and outcrop samples (e.g. Flawn 1956, Muehlberger et al. 1967, Denison and Hetherington 1969, Reed 1993)

and indirect measurements obtained by potential field (gravity and magnetic) methods (e.g. Keller et al. 1980, Adams and Keller 1996). Basement structure has been shown to exert fundamental controls on basin development, determining sedimentation patterns, thermal maturation, and uplift and subsidence (Adams and Keller 1996).

Figure 2.1 – Present-day Geology of the Permian Basin

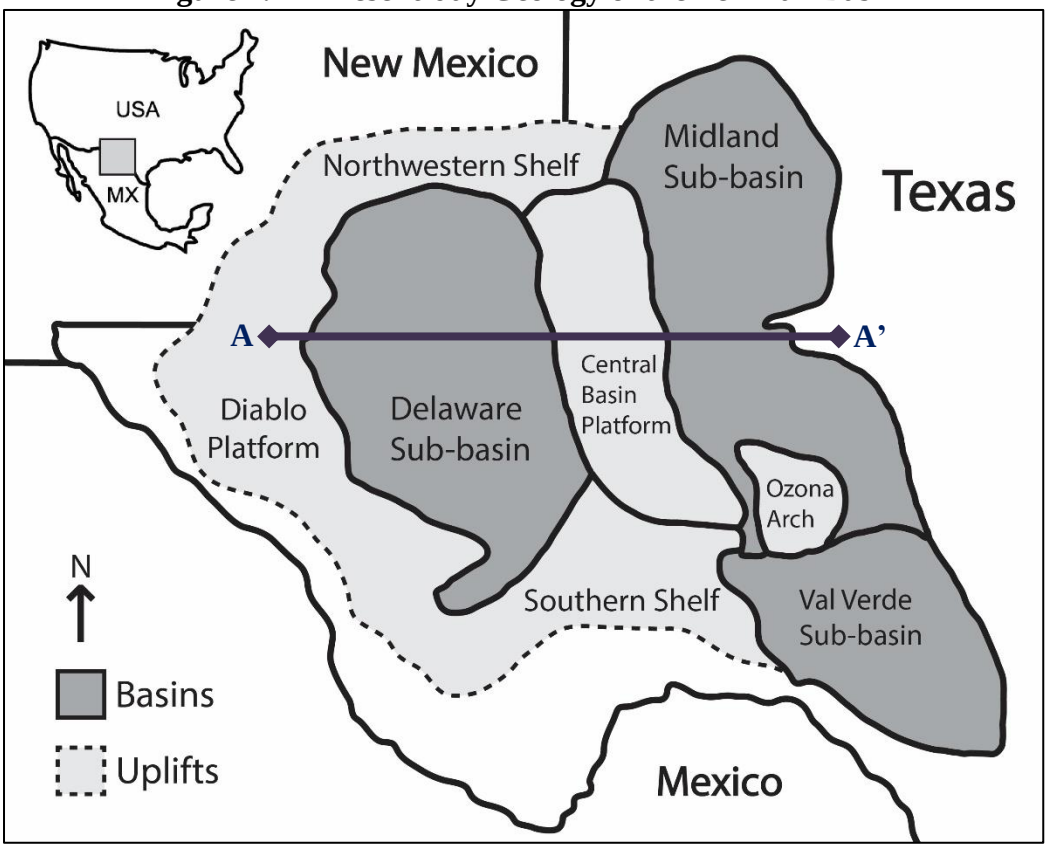

The Permian Basin is sub-divided into numerous sub-basins separated by uplifts. The Delaware and Midland Sub-basins are the largest sub-basins which are separated by the Central Basin Platform, an uplifted basement block. Figure modified from Adams and Keller (1996). The cross-section line A-A' is displayed in Figure 2.2.

Lithospheric strength variations across a region has a direct impact on determining basin geometry and hence hydrocarbon generation, maturation, and migration. Estimation of the effective elastic thickness provides an aggregate, or spatially-averaged, determination of the strength of the lithosphere across a region. Such an estimate enables interpretations to be made

regarding the regional flexure, which is itself a determining factor in shaping foreland basins. More importantly, estimating the effective elastic thickness is the first step in establishing an evolutional model describing the tectonic and structural history of the region. It is especially important to understand the structural framework of the Permian Basin because its tectonic and sedimentation history has direct implications for the entire petroleum system. While it is beyond the scope of the project to interpret finer scale basement features, results from this study may help constrain the importance of geologic structures in either strengthening or weakening the lithosphere, leading to a more comprehensive analysis of basins worldwide.

Figure 2.2 – Generalized Cross-section of the Permian Basin

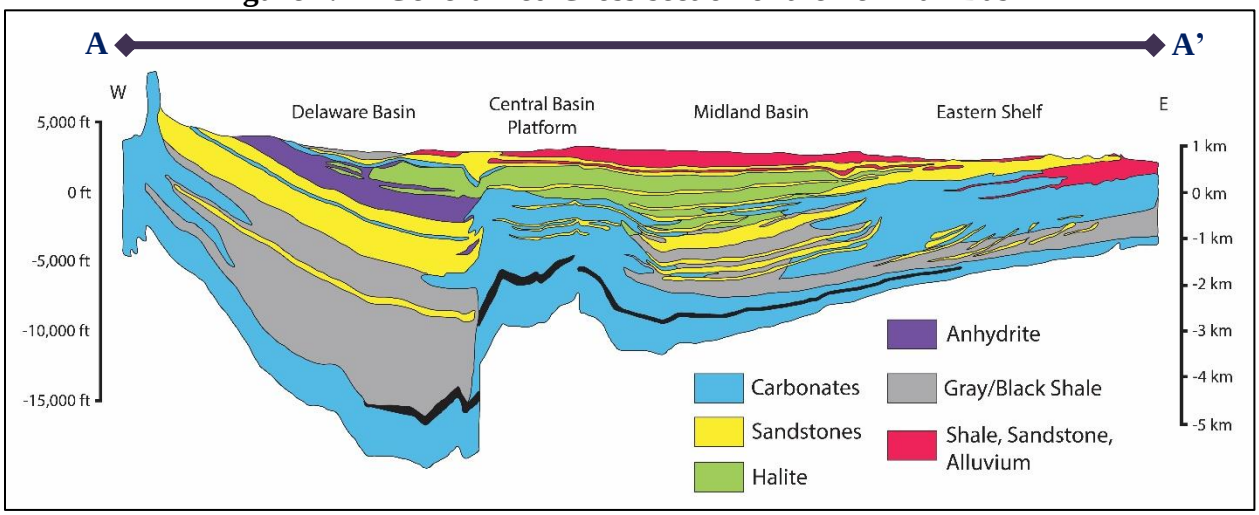

Differentiation of the Tobosa Basin into numerous Sub-basins beginning in the Mississippian created more complex sedimentation patterns. Sandstones, shales, and carbonates characterize the deeper strata while evaporites cap the formations near the present-day surface. Original figure modified from Engle et al. (2016). The spatial extent of the cross-section line A-A' is shown in Figure 1.1.

2.2 Tectonic History of the Permian Basin

Prior to the assembly of Pangea through collision of Laurentia and Gondwana in the late Paleozoic, the Permian Basin was characterized by a broad topographic depression along the southwestern margin of the North American craton, named the Tobosa Basin (TB) or Ancestral

Permian Basin (Galley 1958). Little is known about the region during this time, but it has been hypothesized that the TB formed through crustal extension emanating from a failed triple-junction in the Proterozoic (Walper 1977, Keller et al. 1980, Hills 1984, Adams and Keller 1996). The earliest record of sedimentation in the TB is ascribed to the Late Cambrian. Terrigenous sandstones were deposited on top of granitic basement followed by regionally uniform carbonate deposition during the Late Cambrian to Early Ordovician (Hills 1984). Deformation during the Cambrian to Middle Mississippian is limited to zones of broad, epeirogenic uplifts and depressions (Hills 1985, Horak 1985).

Beginning in the Middle to Late Mississippian, the early stages of continental collision between Gondwana and Laurentia began to deform the TB through reactivation of pre-existing zones of weakness that were inherited from earlier episodes of late Precambrian faulting (Hills 1970, Adams and Keller 1996). Continuation of the continental collision resulted in the Ouachita Orogeny during the Pennsylvanian, culminating in the Ouachita-Marathon Thrust Belt (OMTB) that extends through Arkansas, Oklahoma, Texas, and northern Mexico (Wickham et al. 1976, Pindell 1985, Viele and Thomas 1989). The associated deformation divided the broad, low-lying TB into numerous sub-basins (e.g. Delaware and Midland Basins) separated by uplifts (e.g. Central Basin Platform). Sedimentation patterns became more complex as a result of basin differentiation. The region from this point onward is referred to as the Greater Permian Basin (or simply Permian Basin) characterized by a number of smaller, deeper, asymmetric sub-basins (Hoak et al. 1998).

Intra-continental stresses during the Ouachita Orogeny induced slip along fault planes (Gardiner 1990a, Gardiner 1990b). The main phase of uplift along the CBP occurred during the Middle Pennsylvanian and partitioned the central zone of the TB into the Delaware and Midland Basins (Keller et al. 1980, Hoak et al. 1998). Rapid regional subsidence driven by flexural

compensation of the OMTB topographic load occurred simultaneously with the uplift of the CBP and continued until the Early Permian (Yang and Dorobek 1995a, Yang and Dorobek 1995b, Ye et al. 1996). Thickening of sediments along the margins of the CBP from the Late Pennsylvanian to Early Permian suggests that it acted as an additional topographic load on the region, affecting the flexural and stratigraphic profiles of the Delaware and Midland Basins (Yang and Dorobek 1995b). Basin subsidence and uplift of the CBP ceased in the Late Permian during a period of reduced tectonic activity (Yang and Dorobek 1995a, Hoak et al. 1998). The Permian Basin is thereafter characterized by low subsidence rates that persisted until the beginning of the Cenozoic (Keller et al. 1980, Hills 1984). The only notable structural change during this period is a gradual deepening of the DB accompanied by a slight eastward tilt in the direction of the CBP (Keller et al. 1980).

Throughout most of the Mesozoic the PB was characterized by a stable platform phase wherein the regional structural elements acted as a mechanically integrated unit (Horak 1985). Subduction of oceanic plates beneath the North American craton during the late Cretaceous initiated the Laramide and Sevier Orogenies and deformed much of the western region of North America. The associated orogenic processes formed the Delaware and Guadalupe Mountains which extend into the western PB margin (Horak 1985). As a result, the Permian Basin experienced uplift of its westernmost portions while the eastern side of the DB tilted downward along the CBP margin (Hills 1963, Keller et al. 1980).

During the Cenozoic Era, the Permian Basin was characterized by additional epeirogenic uplift of the western portion of the DB, resulting in the presently observed SE regional dip (Horak 1985). The stress regime shifted from compressional to tensional with deformation limited mainly to normal faulting (Muehlberger et al. 1978). Crustal extension along the Rio Grande Rift resulted

in widespread volcanism throughout the Trans-Pecos region of Texas, i.e. west of the Permian Basin and along the western margin of the DB (Henry and Price 1985, Henry and Price 1986, Henry et al. 1991). The anomalously high heat flow within DSB has been attributed to Cenozoic magmatism and may have contributed to the favorable maturation of hydrocarbons (Horak 1985).

CHAPTER III

TE IMPORTANCE AND ESTIMATION TECHNIQUES

3.1 Lithospheric Properties and Te Trends

The effective elastic thickness (Te) of a lithospheric plate is the thickness it would possess if governed by a purely elastic rheology. Te is used to describe the overall strength of the lithosphere and serve as a proxy for flexural rigidity (D), a parameter which measures the deformability or stiffness of a material under stress. The magnitude of D determines the amount of bending that an elastic plate would experience under an applied vertical load where higher values of D correspond to a more rigid material. The flexural rigidity parameter is related to effective elastic thickness according to Equation 3.1 (Love 1906).

Equation 3.1 – Effective Elastic Thickness

$$D = \frac{ET_e^3}{12(1-v^2)}$$

Where E is Young's modulus and v is Poisson's ratio.

Utilization of Te to describe plate strength simplifies complex subsurface rheologies (plastic, viscous, etc.) to a single parameter and serves as a convenient measure for comparing different plates of various properties and rigidity. Because effective elastic thickness is purely a geometric measure describing the integrated strength of a plate, it does not necessarily represent a depth to a physical boundary within the lithosphere. Previous studies however have revealed relationships between Te and the mechanical and thermal properties of the lithosphere (e.g. Watts 1978). While oceanic lithosphere shows the clearest relationships between Te estimates and

subsurface properties, correlations between Te and the properties of continental regions are important in understanding the long-term mechanical behavior of the lithosphere.

Many early studies focused on the flexure of oceanic lithosphere. Estimates of Te using the elastic plate model were made from shipborne 1-D gravity measurements acquired along relatively isolated geologic features such as the Hawaiian-Emperor seamount chain (e.g. Walcott 1970b; Watts 1978). The advantages of studying oceanic rather than continental lithosphere were evident to early authors; oceanic crust is much less heterogeneous in composition, younger in age, and lacks the complex geologic history and deformation associated with older continental lithosphere. The relative isolation of loading events within oceanic lithosphere also simplifies flexural studies by limiting the presence of boundary loads caused by regional-scale tectonic forces.

The primary factors influencing flexural profiles in oceanic regions are the geometry of the load, the magnitude of the load, and flexural rigidity of the plate (Watts 1978). Plate rigidity in oceanic regions is controlled primarily by its thermal age, i.e. the length of time required for the lithosphere to attain its present-day thermal state under the assumption that the oceanic crust was initially magmatic (Burov and Diament 1995). As oceanic crust ages and migrates farther from the mantle upwelling zone at mid-ocean ridges (MORs), it cools and increases in rigidity, resulting in higher Te estimates (Caldwell and Turcotte 1979). Previous studies have correlated elastic thickness estimates with thermal boundaries, approximating Te to the 450°C isotherm (Watts et al. 1980). Watts (2001) combines 186 Te estimates from 48 previous studies to highlight this relationship. Over 75% of all Te estimates fall within the 300 – 600°C isotherms with exceptions near fracture zones and deep trench systems. Thus, in the absence of thermal anomalies, Te

estimates of oceanic lithosphere reflect not only its integrated strength but serve as a measure of its thermal age.

The age of the oceanic lithosphere at the time of a loading event also affects plate strength (Caldwell and Turcotte 1979, Lago and Cazenave 1981). Younger crust is warmer and less able to support equivalently-sized loads as older, more rigid crust. The weakness of younger oceanic crust corresponds to lower Te values while higher values correlates to older crust at the time of loading. This correlation has allowed authors to constrain both the age of oceanic volcanoes and the timing of thermal rejuvenation of oceanic crust due to mantle heating (Calmant et al. 1990). Regardless of the age of the lithosphere on which they are emplaced, older seamounts and oceanic islands display on average lower values of Te (e.g. Watts 2001). Old oceanic crust which normally would display a high Te value is found to express a lower value if the load is also geologically old. This observation suggests that a *stress relaxation time* occurs whereby loads continuously subside and displace the viscous asthenosphere. Long-lived loads on old oceanic lithosphere therefore weaken the plate and yield lower Te estimates than those observed from old oceanic lithosphere with comparatively younger loads.

Viscoelastic plate models have been utilized in oceanic regions to better explain observed flexural profiles, overcoming some of the limitations of the purely elastic plate model (e.g. Walcott 1970a, De Bremaecker 1977, Lambeck and Nakiboglu 1981). The viscoelastic model helps to explain through forward modelling some of the short-term subsidence that is related to flexure. However, the long-term stability of the lithosphere is likely controlled more by elastic rather than viscous properties, as evidenced by the continuous support of loads for long periods of geologic time (Watts 2001). Viscoelastic models therefore tend to overpredict flexure for long-term loads and consequently underestimate elastic thickness estimates determined from spectral studies.

An important development used in conjunction with elastic thickness estimates is the Yield Stress Envelope (YSE). The YSE quantitatively distinguishes how different crystalline structures and compositions respond to laboratory stress conditions and combines brittle and ductile deformation laws determined via rock deformation experiments into a single strength profile for the lithosphere (e.g. Byerlee 1978, Goetze and Evans 1979). However, strain rates in deformation experiments are orders of magnitude higher than those in real world conditions. Nevertheless, the YSE combines strain rates, stress, and temperature in both tensional and compressional settings to model how rocks behave in the subsurface. The strength profiles modelled by the YSE predict the maximum differential stress that can be supported by rocks as a function of depth. The depth dependence of rock strength incorporates multiple factors such as pressure, temperature, structures, and fluid content which determines the particular shape of the yield curves. Because the maximum stress difference that the lithosphere can support is indicative of its strength, the area under the YSE provides a measure of the integrated strength of the lithosphere. YSEs are often utilized to validate rock mechanic data, explain the mechanical behavior of the lithosphere, and predict failure mechanisms based upon depth, temperature, and composition (Burov 2011). In regions where the lithosphere has yielded through brittle or ductile deformation rather than flexed, the YSE can be used to predict the "true" value of Te by comparing observations of flexure with calculations based upon its YSE (Lavier and Steckler 1997). The amount of plate yielding can then be quantified and a more realistic value of Te obtained.

Figure 3.1 – Example Yield Strength Envelope (YSE) for Continental and Oceanic Regimes

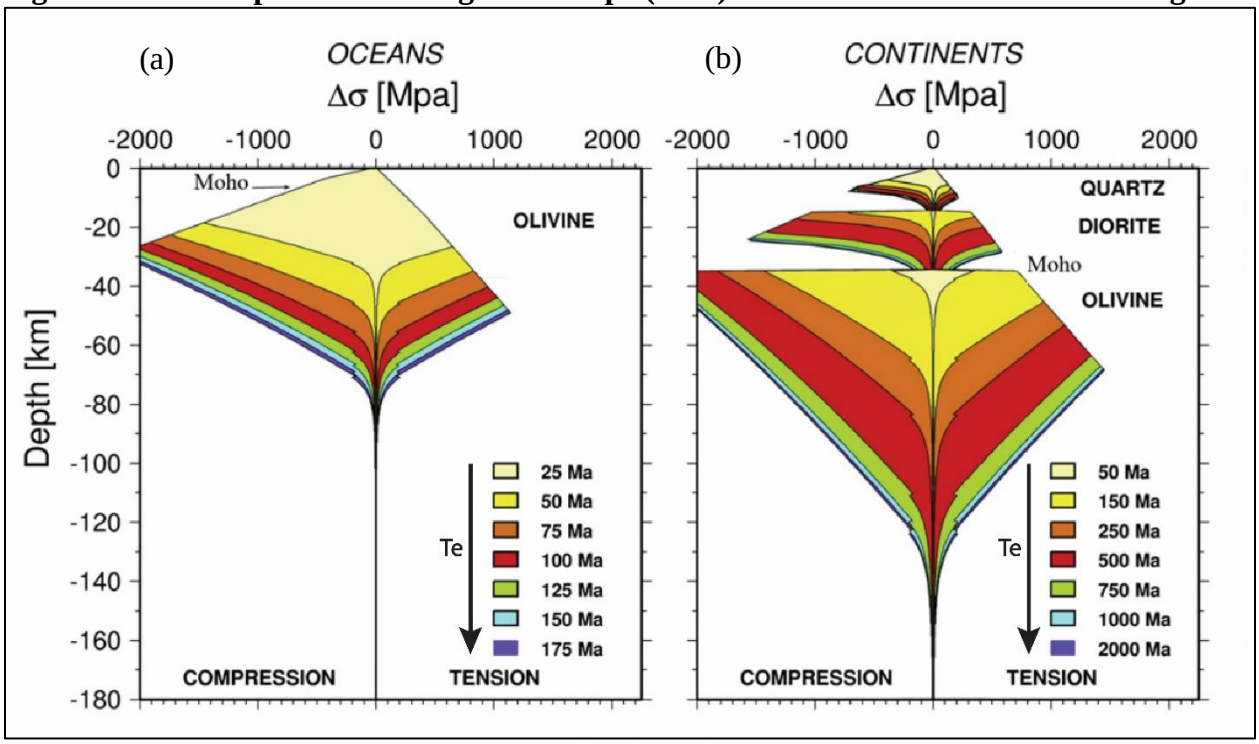

Strength profiles are plotted as a function of thermo-tectonic age as lithospheric strength correlates closely to the amount of time elapsed since the last tectonic event. The linear portions of the YSE are determined via Byerlee's law (Byerlee 1978). The curved portions represent ductile deformation as strength exponentially decreases due to increased temperatures (Burov and Diament 1995). **(a)** The oceanic region has a single ductile transition zone due to its homogeneous composition. **(b)** Continental regions display a multi-layered structure which can lead to mechanical decoupling of the lower crust with the upper mantle. A return to brittle failure characterizes continental regions due to a change in composition from Diorite to Olivine. Figure modified from Burov (2011).

Flexural studies of continental lithosphere are notably more difficult than their oceanic counterparts. The increased age of continental crust results in inherited deformational and compositional heterogeneities that can control present-day plate strength (e.g. Audet and Burgmann 2011). The presence of these inherited features implies two important considerations: (1) Te magnitudes reflect not only present-day flexure but also contains information regarding historical structures and deformation and (2) loading events are rarely isolated on continental lithosphere. The former implication can be used to constrain a region's history with spatially-varying Te maps while the latter restricts our interpretations. More specifically, flexural profiles

are often modified by geologic processes beyond a geographically-located study area which can in turn bias elastic thickness estimates. Te values are obtained through spatially-finite data windows that often do not include the effect of boundary loads. If such loads are important, the flexural profile of the study region may be altered and spectral analysis studies which do not include the effect of boundary loads can yield inaccurate Te estimates.

The presence of strong horizontal stresses also affects flexural profiles and can produce inexact Te values if not considered. Regions under compression (e.g. plate margins during collisional events) often overcompensate topographic loads with increased flexure, reducing the apparent plate rigidity which results in erroneously low Te estimates (Stephenson and Lambeck 1985a). Forward modelling of lithospheric mechanics can be used to constrain Te magnitudes, but the inability to account for spatially varying mechanical properties (e.g. flexural rigidity D) is inherent in studies that transform data to the wavenumber domain (e.g. Crosby 2007). In general, the dependence of Te estimates on inherited features and poorly constrained boundary conditions makes it difficult to quantify the mechanical and thermal properties of continental lithosphere.

The difficulty of characterizing lithospheric properties from elastic thickness estimates is summarized in Watts (2001). Trends associated with plate age, load age, Te magnitudes, and model parameters such as flexural rigidity are evaluated based on 48 prior studies comprising 75 separate Te estimates. Watts demonstrates that plate rigidity does not depend on a single parameter such as thermal age. Neither is there a clear relationship between Te values and the age of loading, nor can a single relaxation curve for a viscoelastic model be used to explain the wide variety of continental Te values. While thermal structure has been shown to play a critical role in determining flexural rigidity, thermal properties are themselves controlled in an uncertain manner by other

factors such composition, lithospheric thickness, and mantle convection (Burov and Diament 1995; Sahagian and Holland 1993).

Other authors have discovered correlations between lithospheric strength of continental regions and thermo-tectonic age, defined as the elapsed time since the last tectonic event (Poudjom Djomani et al. 1999). Defined in this manner, thermo-tectonic age is synonymous to plate age for oceanic lithosphere. The relationship between thermo-tectonic age of continental lithosphere and elastic thickness estimates suggests that Te values can be used to constrain a region's most recent tectonic history along with its present-day thermal properties. Sahagian and Holland (1993) showed that elastic strength and thermal structure is controlled by lithospheric thickening or thinning. Lithospheric thinning events are primarily associated with rifting and lead to reduced plate rigidity due to increased heating from the mantle. Continental collision is the primary mechanism for lithospheric thickening whereby both the crust and lithospheric mantle shorten, increasing the overall thickness of the lithosphere. A thicker lithosphere in turn reduces surface heat flux and increases plate rigidity. Conduction from the mantle and radiogenic heating of crustal isotopes will equalize the thermal state of the lithosphere which increases surface temperatures and weakens the plate through time. Thus, lithospheric strength becomes a time-dependent process after a tectonic event before reaching a steady state determined by the plate's original thermal structure and the amount of lithospheric thickening or thinning (Sahagian and Holland 1993).

Elastic thickness magnitudes can also be used to investigate large-scale tectonic features and structural trends beyond the resolution of seismic surveys and drilling data. Previous studies have revealed that Archean cratons possess great strength while Phanerozoic continental margins are characterized often display significant weakness (Hartley 1995). Perez-Gussinye and Watts (2005) utilized geophysical modelling to arrive at similar conclusions, attributing the strength

difference between old and young continental lithosphere to a change in plate structure as mantle temperatures and volatile content decreases through time. These processes result in a lower geothermal gradient and increased lithospheric rigidity. Their conclusions support previous work by Poudjom Djomani et al. (1999) and imply that lithospheric strength is partially inherited from previous tectonic and thermal events. Other geologic studies have independently observed this phenomenon (e.g. Jordan 1978) whereby cratons tend to preserve their strength during supercontinent cycles while continental margins are repeatedly weakened and hence preferentially deform in future cycles.

Audet and Burgmann (2011) developed a global map of Te using 2-D gravitational coherence (see Section 3.5) to show that elastic thickness magnitudes are high in Archean cratons but low in the surrounding Proterozoic margins (Figure 3.2). Their study supports the idea that lithospheric rigidity is controlled by inherited structures from previous geologic events. During supercontinent cycles, strain and deformation is concentrated at pre-existing zones of weakness along continental margins while cratonic interiors resists much of the deformation. Their study also reinforced previous notions that Te varies with thermo-tectonic age, and that these major events reset the lithosphere's strength through large-scale vertical convection of the mantle during continental assembly and breakup. These processes occur simultaneously with margin-wide faulting and fault reactivation that induces mechanical anisotropy such that future tectonism preferentially deforms continental margins by concentrating strain at pre-existing structures. Over time these forces have isolated continental interiors which exhibit significantly greater strength than continental margins.

Figure 3.2 – Global 2-D Coherence Study by Audet and Burgmann (2011)

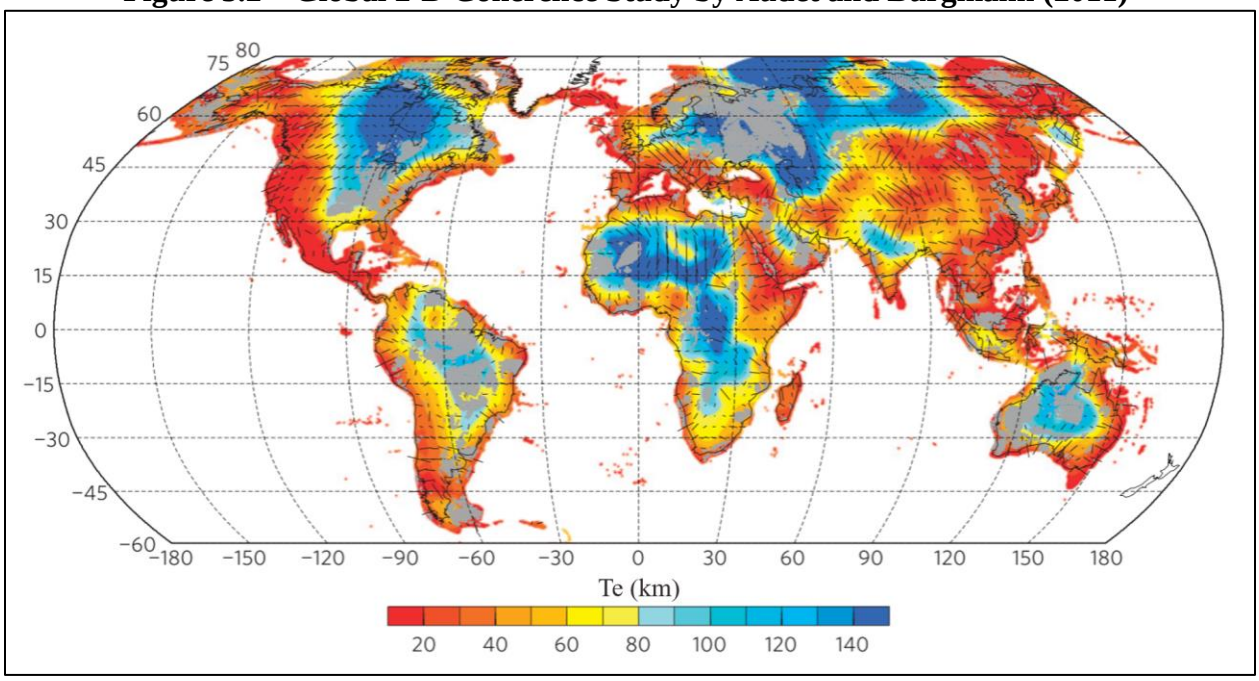

Warm colors correspond to low Te values and thus a weak lithosphere. Cooler colors represent high Te values and a stronger lithosphere. Oceanic lithosphere is predominantly weak due to its relatively young geologic age while old continental lithosphere displays greater strength. The length and orientation of the small black lines represents the magnitude and direction of the maximum value of Te anisotropy, respectively. Te anisotropy is not explored in this study. Figure modified from Audet and Burgmann (2011).

A more recent study by Mouthereau et al. (2013) utilized their own global Te map to show that inherited lithospheric strength influences not only the style of deformation but also the amount of shortening during orogenic events (Figure 3.3). They identify mantle strength as the major control in determining the amount of shortening and the total deformation. Low values of Te correspond to a weak lithospheric mantle which subsequently increases the amount of deformation by activating deep basement features during collisional tectonic events. Ductile deformation dominates the weak mantle model. Strain is concentrated in a relatively small geographic area which displays on average less shortening. The mechanism for increased shortening for the strong mantle model is attributed to generation of a shallow-dipping detachment surface. Deformation is

concentrated mostly along the décollement which reduces the overall regional deformation but increases the amount of shortening as features are able to easily slide past one another.

Figure 3.3 – Global 2-D Coherence Study by Mouthereau et al. (2013)

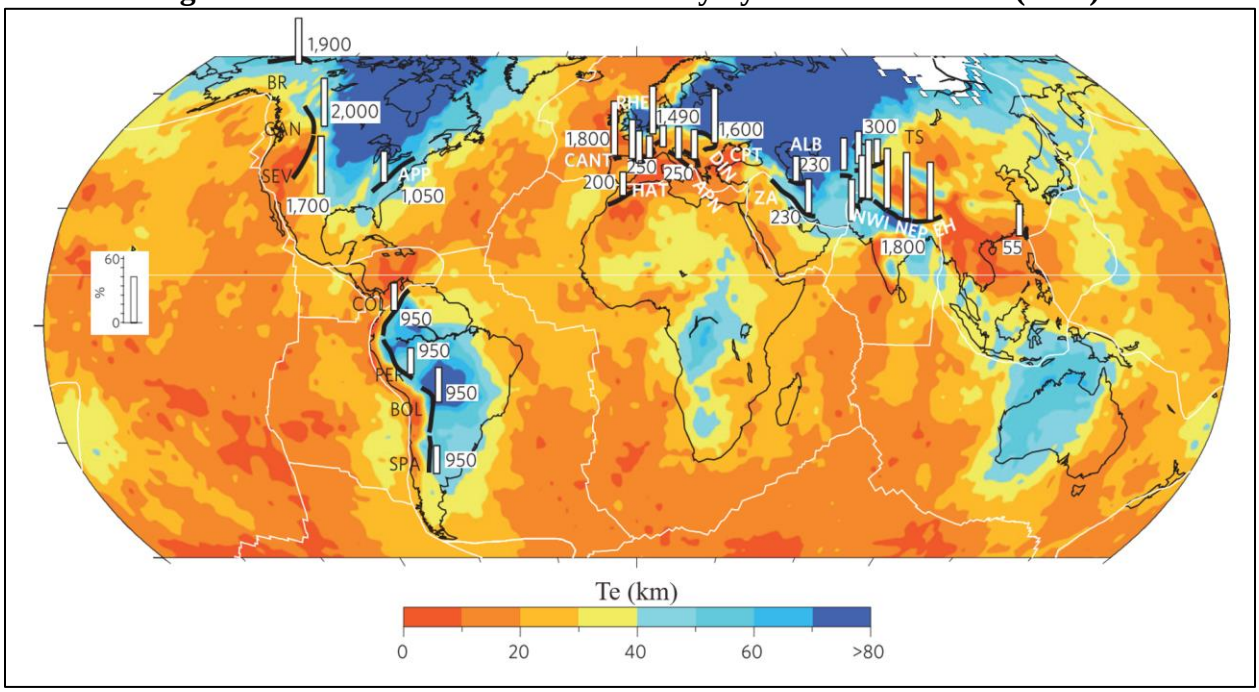

Warm colors correspond to low Te values and thus a weak lithosphere. Cooler colors represent stronger lithosphere. Vertical bars represent the degree of shortening in along orogenic collisions zones which are shown with bold, black lines. The numerical value next to the vertical bars represents the mean thermo-tectonic age (Myr) of the collisional zone. The general trend of continental margins and oceanic lithosphere having lower Te values while cratons display significantly higher Te estimates is similar to that of Audet and Burgmann (2011). However, Te magnitudes for each of these studies are not the same due to different methods of processing gravity and topography data. Figure modified from Mouthereau et al. (2013).

Modelling by Burov and Watts (2006) stressed the importance of the lithospheric mantle in controlling deformation styles. Their study showed that a strong upper mantle is required to support long-term surface loads. A weaker mantle represented by low values of elastic thickness is mechanically unstable and tends to decouple from the crust in compressional settings. Such a model is often referred to as the "crème brûlée" model and characterizes regions which experience increased Moho temperatures and a collapse of surface topography as the lithosphere is thermally weakened and becomes incapable of supporting long-term loads. Burov and Watts concluded that

the crème brûlée model does not fit observed flexural profiles. Rather, the "jelly-sandwich" model is preferred wherein lithospheric strength is supported by both the crust and uppermost mantle. Thus, continental strength, represented in effective elastic thickness estimates, influences not only the stability of orogenic events but also reveals important information regarding thermal and mechanical properties of the lithospheric mantle.

The YSE has been applied to continental regions (e.g. Karner and Watts 1983, McNutt et al. 1988), though its application is more difficult than in oceanic regions (see Figure 3.1). Greater compositional heterogeneity, increased lithospheric thickness, poorly constrained geothermal gradients, and variable strain rates complicates the analysis. Despite the uncertainties, the YSE has proved to be crucial in predicting a crust-mantle decoupling which is used to explain the extraordinarily low Te values observed in regions of extensional and compressional stress regimes (McNutt et al. 1988). Burov and Diament (1992, 1995) developed an analytical model that relates the strength of the YSE to elastic thickness estimates. Their model provides rheology-consistent explanations for the behavior of Te in both continents and oceans and reveals that lithospheric strength is controlled by a combination of its thermal structure, crust-mantle coupling state, and bending stresses imposed by flexure of geologic loads.

Of special importance to this project is a study performed by Lavier and Steckler (1997) who used a parameterization of the YSE that includes the effects of crust-mantle decoupling to explain low estimated Te values in foreland basins. Young, hot lithosphere can overcome yield stresses through bending and decouple the rigid crust from the weakened mantle. Older lithosphere which displays greater strength often remains coherent. Lavier and Steckler (1997) also demonstrated the importance of sedimentary cover in reducing the flexural strength of continental lithosphere. Deposition and subsequent loading of low-density, low-thermal-conductivity

sediments within foreland basin depocenters insulates the lower crust, thereby increasing temperatures and lowering the yield strength (Steckler and Brink 1986, Lavier and Steckler 1997). The decreased yield strength critically weakens the plate and allows for crust-mantle decoupling which then explains low Te values observed in such regimes.

Even accounting for variability in the thermal state of lithosphere, the range of elastic thickness estimates in continental regions is notably high, ranging from less than 5 km to greater than 120 km (Watts 2001). The range can be partially explained by uncertainties and ambiguities in the application of various inversion techniques (e.g. admittance and coherence) and plate models (e.g. viscoelastic, elastic, elastic-plastic). Model parameters such as flexural rigidity, Poisson's ratio, and Young's modulus also affect inversion results and their uncertainties have been shown to cause a 10-20% variation in Te estimates (Burov and Diament 1995). Burov and Diament (1995) propose that a 25% uncertainty factor exists for all continental Te estimates. Nevertheless, the use of Te has been valuable in understanding the tectonic and thermal evolution of continental regions and remains a fundamental measure of lithospheric strength and reveals important information regarding mechanical properties, isostatic state, and thermal history.

3.2 Observed Admittance Function

Gravitational admittance is a wavenumber function that contains information on a region's isostatic state and allows for estimations of Te to be made through comparison of the observed admittance function with theoretical plate models (Watts 2001). Mathematically, admittance is a linear transfer function that, when convolved with the topographic signal in the spatial domain, predicts the gravity anomaly signal (Lewis and Dorman 1970) (Equation 3.2). In this respect,

gravitational admittance is a linear filter containing terms that describe geologic properties of the subsurface (e.g. Watts 2001, Kirby 2014).

Equation 3.2 – Admittance in the Spatial Domain

$$g(x) = z(x) * h(x)$$

Where g(x), h(x), and z(x) are the spatial domain signals of the gravity, topography, and admittance functions respectively, and the star operator ($*$) represents a convolution process.

Rather than attempting to design an inverse filter to deconvolve the topography signal from the gravity signal in the spatial domain, early studies utilized spectral analysis, namely Fourier analysis (e.g. McKenzie and Bowin 1976, Watts 1978). In the spatial frequency domain, also called the wavenumber domain, deconvolution becomes a simple division operation of the gravity signal by the topography signal, yielding the observed admittance function (Equation 3.3).

Equation 3.3 – Admittance in the Wavenumber Domain

$$\mathbf{Z}(k) = \frac{\mathbf{G}(k)}{\mathbf{H}(k)}$$

Where k is the wavenumber ($k = 2\pi / \lambda$ with λ representing the wavelength) and $\mathbf{G}(k)$, $\mathbf{H}(k)$, $\mathbf{Z}(k)$ are the wavenumber functions with bold, capital letters representing the Fourier transforms of their corresponding spatial domain functions (see Equation 3.1).

To minimize the presence of noise that inherently exists in the wavenumber representations of the signals and the "geologic noise" not representative of flexure, the observed admittance is calculated using cross-spectral techniques proposed by Munk and Cartwright (1966). McKenzie and Bowin (1976) formulated an admittance function with a higher signal-to-noise ratio by dividing the cross-spectrum of the topography and gravity signal by the power spectrum of the

topography signal (Equation 3.4). Calculation of the observed admittance results is a complex-valued function. However, the elastic plate model only predicts reveal values for the theoretical admittance functions. Thus, only the real values of the observed admittance are utilized in its calculation (Kirby 2014).

Equation 3.4 – Normalized Admittance in the Wavenumber Domain

$$\mathbf{Z}_{\mathrm{obs}}(\mathrm{k}) = \frac{< \mathbf{G}(\mathrm{k})\mathbf{H}^{*}(\mathrm{k}) >}{< \mathbf{H}(\mathrm{k})\mathbf{H}^{*}(\mathrm{k}) >}$$

Where $\mathbf{H}^{*}(\mathrm{k})$ represents the complex conjugate of the wavenumber domain topographic function $\mathbf{H}(\mathrm{k})$. Angle brackets denote a smoothing process of the admittance function. The star operator ($*$) represents a convolution process.

Additionally, McKenzie and Bowin (1976) developed an averaging process to further reduce noise in the admittance function by dividing the long ship profiles into numerous equal-length profiles and then averaging their spectra. However, the sub-profiles cross different geologic features which biases the overall admittance function. An improved averaging process was performed by Watts (1978) in which multiple profiles across a single geologic feature were averaged in the wavenumber domain. This averaging method, herein considered the Watts' Method, allows for a better regional expression of flexure to be found in the admittance function and helps improve effective elastic thickness estimations through inversion. The Watts' Method has been adopted and modified further for the purposes of this study (see Section 4.4).

3.3 Theoretical Admittance and the Elastic Plate Model

Theoretical admittance curves are derived through the modelling of the lithosphere as various forms of viscoelastic and elastic plates. The derivation of the multifarious plate models is

a laborious and difficult process, and only a brief overview of the elastic plate derivation is included herein to orient the reader and allow for discussion of model failures. Watts (2001) and Kirby (2014) have provided a thorough review of the derivation process.

The elastic plate model assumes a thin elastic plate (in one or two-dimensions) is placed upon an inviscid substratum (taken to the be asthenosphere), whose deflections are small compared to the overall thickness of the plate, and whose thickness is small compared to its lateral extent (assumed to be infinite). This model also assumes that stresses in the plate during bending are linearly proportional to strain, simplifying the mathematics involved and allows for the principle of superposition to be utilized which allows flexure due to a load to be computed from the sum of its component loads. The elastic model simplifies the complex, multi-layered rheologies of the lithosphere to an equivalent elastic plate that is rheology-independent whereby the estimated effective elastic thickness is a measure of the integrated strength and proportional to its flexural rigidity (Banks et al. 1977; Watts and Burov 2003). The elastic plate model however can store an infinite amount of stress without fracturing or yielding to plastic deformation (Watts 2001). While this is not necessarily geologically reasonable, the elastic plate model has seen the most widespread application due to its simplicity and has been used been used a reference model for flexural studies and Te estimates (Watts 2001).

Deriving the theoretical curves for the gravitational admittance function requires a return to material science. Timoshenko and Woinowsky-Krieger (1959) provide the second-order partial differential equation relating the deflection of an isotropic, thin, rectangular, elastic plate subjected to a vertical load. Bending and twisting moments of the elastic beam are specified within this equation, which are then defined by functions relating the moments to deflections (Burov and Diament 1995). Transformation of this combined equation into the wavenumber domain via

Fourier transform requires that flexural rigidity (D) be held constant. As outlined in Banks et al. (1977), the wavenumber domain transformation yields one which relates the deflections of the plate, buoyancy forces as the plate displaces the underlying fluid, and the applied initial load (Equation 3.5).

Equation 3.5 – Wavenumber Domain Deflections

$$\mathrm{D}k^4\mathbf{W}(k) + \mathbf{P}(k) = -\mathbf{L}(k)$$

Where k is the wavenumber, $\mathbf{W}(k)$ is the deflection, $\mathbf{P}(k)$ is the buoyancy force, $\mathbf{L}(k)$ is the applied initial load, and D is the flexural rigidity function (see Equation 3.1).

Green's Equivalent Layer Theorem is applied to determine the surface-measured gravity anomaly which would exist after flexure of an elastic plate (Kirby 2014). Karner (1982) and Karner and Watts (1982) provide the first order approximation of the gravity anomaly function (Equation 3.6).

Equation 3.6 – Green's Equivalent Layer Theorem

$$\mathbf{G}(k) = 2\pi\gamma(\rho_m - \rho_c)e^{-kz}\mathbf{W}(k)$$

Where γ is the Newtonian gravitational constant, ρ_m is the density of the mantle, ρ_c is the density of continental crust, z is the depth to the layered deflection, and $\mathbf{W}(k)$ is the wavenumber deflection function.

In flexural models, Equation 3.5 is used to determine the final surface topography after flexure, and Equation 3.6 is used to determine the resulting gravity anomaly. These equations are then used to determine the theoretical admittance functions for various loading cases. Watts (2001) provides derivation of the wavenumber functions necessary to model theoretical admittances for

three different loading schemes: (1) surface loading (Equation 3.7), (2) buried loading, and (3) combined surface and buried loading (Forsyth 1985). The loading case considered for this project is surface loading only, chosen after initial modelling of the admittance functions across the Permian Basin revealed that the surface loading scheme best fits the data.

Equation 3.7 – Theoretical Admittance with Surface Loading for a Thin Elastic Plate

$$\mathbf{Z}(k) = -2\pi\gamma\rho_c e^{-kZ_t}\left(\frac{Dk^4}{g(\rho_m + \rho_c)} + 1\right)^{-1}$$

Where k is the wavenumber, ρ_m is the density of the mantle, ρ_c is the density of continental crust, γ is the gravitational constant, g is the acceleration due to gravity (9.8 m/s^2), Z_t is the mean thickness of the crust, and D is the flexural rigidity parameter.

Theoretical admittance functions are plotted in Figure 3.4 using Equation 3.7. As stated in Section 3.2, the admittance is a linear transfer function that predicts the gravity anomaly from the topography signal. Alternatively stated, the admittance measures the degree of agreement between the gravity and topography signals at given wavenumbers. Admittance at low wavenumbers (long wavelengths) approaches the same magnitude for all values of Te. Conceptually this can be understood by considering the degree of agreement between the long wavelength components of the gravity anomaly and topography signals. The lithosphere, regardless of its strength, is unable to support long wavelength, high amplitude topographic loads (e.g. mountain belts) and will result in compensation at depth by flexure of the lithosphere. High wavenumber (short wavelength) topographic loads are supported by the strength of the lithosphere and thus do not correlate with the Bouguer gravity anomaly at these wavenumbers. Hence, the agreement between the signals is low which results in low magnitudes of admittance.

Figure 3.4 – Theoretical Admittance Functions with Surface Loading

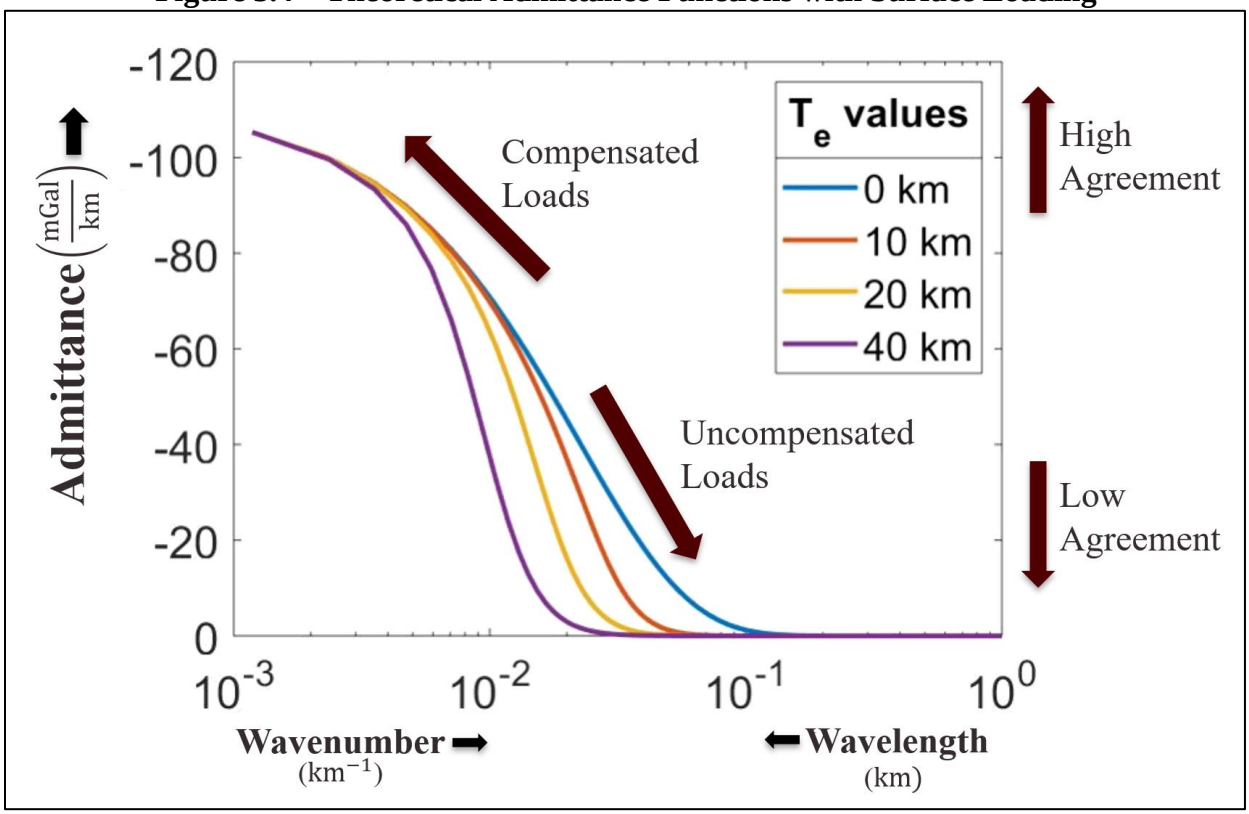

Four theoretical admittance curves for a thin elastic plate subject to surface loading are generated utilizing Equation 3.7 and shown in bold, colored lines. Compensated loads are those with long enough wavelength and high enough amplitude (e.g. mountain ranges) to cause the lithosphere to flex. Uncompensated loads are short-wavelength, low amplitude variations in natural topography that are supported by the integrated strength of the lithosphere and do not cause flexure. The rate of transition from compensated to uncompensated loading schemes is determined by the strength of the lithosphere and quantitatively measured by Te.

3.4 Other Plate Models

While the elastic plate model has enjoyed the most widespread application, various other models exist which can be utilized in flexural studies. Viscoelastic plate models (e.g. Walcott 1970a, McNutt and Parker 1978) and derivatives such as linear viscoelastic (e.g. Karner 1982), Maxwell viscoelastic (e.g. Beaumont 1981), elastic-viscoelastic (e.g. Lambeck and Nakiboglu 1981), and multi-layer viscoelastic (Zhong 1997) have been applied to both oceanic and continental regions. Broken plate models have also been used to forward model flexural profiles (e.g. Karner and Watts 1983), though these are limited to the spatial domain. Application of a

continuous plate model to a geologically broken plate will underestimate Te by a small factor and can be used to qualitatively express true lithospheric strength (Lowry and Smith 1995). Thin elastic shells with both uniform rigidity (Turcotte et al. 1981, Lowry and Zhong 2003, Belleguic et al. 2005, Audet 2013) and spatially-varying rigidity (Beuthe 2008) have been derived recently with admittance and coherence equations (Audet 2013), but these functions have not seen widespread application to flexural studies; only the viscoelastic model has seen notable use in continental and oceanic studies.

The advantage of the viscoelastic plate model is that it incorporates both viscous and elastic properties whereby the plate is initially elastic and becomes more viscous as the age of the load increases. The viscoelastic model and its derivatives are visualized with springs and dashpots in series, parallel, or in combinations of the two which determines their respective stress-strain curves. The viscous effects of the model are attributed to asthenospheric properties and are represented by the relaxation time parameter, defined as the time required for elastic strain to equal viscous strain. Because the model responds to vertical stresses initially through elastic deformation and later by viscous yielding, the relaxation time parameter controls the long-term effects of flexural profiles.

Simple, single-layer viscoelastic plate models have been used mainly in oceanic region to account for short-term subsidence (e.g. Watts 1978). However, with only a single value for the relaxation time parameter, the viscoelastic plate model overpredicts flexure for long-term loading events. Consequently, Te values are overestimated in the short term and underestimate plate strength for long-term loading events (Watts 2001). The viscoelastic plate model also increases the difficulty of estimating elastic thickness through inversion. An equivalent elastic plate must be specified with observed flexure of a viscoelastic model prior to estimating Te, and the viscoelastic

plate equations are highly non-linear (De Rito et al. 1986). Additionally, Te estimations utilizing a viscoelastic plate model are dependent upon the age of the load, and prior studies have shown that different relaxation times are needed to explain variations in Te along similarly-placed loads within oceanic lithosphere (e.g. Watts 1978).

The multi-layer viscoelastic plate model was developed to better explain both the short-term and long-term effects of flexure (e.g. Zhong 1997). Utilization of a two-layer model allows for viscosity parameters to be specified for each layer. Viscous effects of the top later characterize the flexure of early-phase loading events while the viscosity of the lower layer determines the long-term effects of the loading on the lithosphere (Watts 2001). A two-layer viscoelastic plate model predicts small subsidence as the thickness of the material that supports the load involves the crust and much of the mantle. As time elapses, viscous effects become more dominant than elastic effects and the load begins to subside. Theoretical modelling of flexure with the two-layered viscoelastic model reveals that high values of viscosity for the upper layer with lower values of viscosity for the base layer is comparable to the predictions of flexure observed in the elastic model and fits well with observed data of long-term loading in oceanic regions (Watts 2001). The multi-layer viscoelastic model however contains non-linear rigidity equations, and inversion with such a model is difficult and ultimately compared to an elastic model when Te magnitudes are estimated.

Viscoelastic models have been applied to continental lithosphere with limited success. Beaumont (1981) utilized a viscoelastic plate model to explain the subsidence, topographic relief, and stratigraphic patterns observed in foreland basins. However, Beaumont's studies were largely unconstrained in loading sizes, which were determined by "trial and error" until a load size and geometry could predict the observed stratigraphic record and present-day flexural profile. Neither could the loads be independently verified with gravity modelling of existing structures. Subsequent

work by Flemings and Jordan (1990), Coakley and Watts (1991), and Sinclair et al. (1991) showed that when more realistic sedimentation diffusion models were used, an elastic plate model could explain the observed stratigraphic record in foreland basins. Additionally, the presence of large-amplitude free-air gravity anomalies over Paleozoic orogenic belts and granites in the Precambrian Shield of North America have been used as an argument that there is no significant viscous relaxation to stresses associated with orogenies (Watts 2001). The elastic plate model also provides a self-constraint explanation of both the gravity anomaly and stratigraphic data and has been widely accepted for foreland basin flexural modelling. Thus, for the purposes of this project, the elastic plate model will be utilized in determining Te estimations.

3.5 Gravitational Coherence

Forsyth (1985) recognized that previous studies which yielded low Te estimates of the continental United States (e.g. Banks et al. 1977) may be underestimating plate rigidity by only considering surface loading. Forsyth derived a new spectral technique to estimate elastic thickness, combining both surface and buried loading schemes provided by Banks et al. (1977) and McNutt (1983) into a wavenumber domain function with a loading ratio parameter describing the relative contribution of buried-to-surface loading. The combined equation predicts the Bouguer coherence curves between gravity and topography whose observed function is given by Equation 3.8. Forsyth's method became the forefront of flexural studies and has remained the most widely used inversion technique for continental Te estimation.

Equation 3.8 – Observed Coherence

$$\boldsymbol{\Gamma}^2_{obs}(\mathrm{k}) = \frac{|< \mathbf{G}(\mathrm{k})\mathbf{H}^*(\mathrm{k}) >|^2}{< \mathbf{G}(\mathrm{k})\mathbf{G}^*(\mathrm{k}) >< \mathbf{H}(\mathrm{k})\mathbf{H}^*(\mathrm{k}) >}$$

Where $\mathbf{G}(\mathrm{k})$ and $\mathbf{H}(\mathrm{k})$ are the gravity and topography signals respectively in the wavenumber domain, $\mathbf{G}^*(\mathrm{k})$ and $\mathbf{H}^*(\mathrm{k})$ are their complex conjugates, k is either the 2-D or 1-D wavenumber, and $\boldsymbol{\Gamma}^2(\mathrm{k})$ is the real-valued coherence. Angle brackets denote an averaging process.

Gravitational coherence is a measure of the phase relationship between the gravity and topography signals and varies between zero and one (Kirby and Swain 2011). Alternatively stated, coherence is a measure of the degree to which gravity anomalies can be linearly predicted from topography (Pérez-Gussinyé et al. 2004). In similarity to gravitational admittance, there exists a spectral window in which coherence shifts from compensated to uncompensated topography, represented by a falloff from a value of one to zero. The wavelength at which the correlation between topography and the Bouguer anomaly falls off is determined by flexural rigidity and hence can be used to estimate elastic thickness. Forsyth's method utilizes the Bouguer gravity anomaly rather than free-air gravity; the calculation of the Bouguer anomaly removes gravitational effects of short-wavelength, uncompensated surface topography, reducing the correlation between topography and the gravity anomaly at high wavenumbers which in turn improves the model's falloff curves.

The reliability of Forsyth's method has been called into question in recent years. McKenzie and Fairhead (1997), McKenzie (2003), and McKenzie (2010) argue that the coherence method yields overestimates of elastic thickness of continental lithosphere in regions of reduced topography, and that Te should not exceed the seismogenic layer thickness (Ts). Additionally, McKenzie and Fairhead (1997) argue that Te values predicted by coherence studies in shield

regions (e.g. Zuber et al. 1989) correspond to depths at which temperatures and pressures are incapable of supporting elastic stresses over geologic timescales. Watts (2001), Perez-Gussinye and Watts (2005), Kirby and Swain (2009), and Perez-Gussinye et al. (2009) do not share these conclusions. They assert that the coherence method accurately estimates elastic thickness and that Te is geologically capable of exceeding Ts.

McKenzie and Fairhead (1997) and McKenzie (2003) investigated the coherence method and challenged the model's underlying assumptions. Forsyth's method assumes that the free-air gravity anomaly and topography are coherent at wavelengths shorter than 500 km. Additionally, the power of the gravity from the uncompensated topography must be comparable to that of the observed gravity at short wavelengths. If these assumptions are not satisfied either because the short-wavelength gravity is dominated by subsurface loads and not by topography, then coherence only provides an upper bound of Te and is not a true estimate. McKenzie and Fairhead (1997) instead used gravitational admittance for shield regions to estimate Te. Their elastic thickness estimates were everywhere less than seismogenic thickness and in agreement with the known rheological behavior of continental lithosphere. McKenzie and Fairhead (1997) also conclude that coherence can only be used to test for compensation at wavelengths greater than 1000 km. This is an important consideration for this study since the maximum signal distance across the Permian Basin for this study is 863 km.

Simons et al. (2000), Banks et al. (2001), and Armstrong and Watts (2001) challenged these conclusions. They argue that McKenzie and Fairhead (1997) neglect the effect of internal loading on topography. However, McKenzie and Fairhead defined gravity anomalies that are not expressed in the topography resulting from internal loading as noise within the observed coherence function. This is an appropriate consideration since Forsyth's model assumes that all loads

generate surface topography and that the coherence between buried and surface loads is zero. McKenzie (2003) demonstrated various theoretical cases in which significant buried loads lack topographic expression. Such cases can be achieved geologically through erosion and sedimentation processes which remove topography and fill depressions, producing a flat landscape while leaving internal loading unaffected. Erosion and sedimentation therefore generate surface loads which are coherent with the internal loads. Forsyth explicitly excluded internal loads that correlate to surface loads from his model, and his expressions will therefore not give the correct value of Te if such loads are important. Crosby (2007) carried out a series of numerical experiments which showed that the value of Te estimated using Forsyth's method is indeed larger than the true value in the presence of such noise.

McKenzie (2003) also concluded that no significant internal loading exists in any of the seven continents which produces topography expression. This implies that surface processes such as erosion and sedimentation either have a strong impact on lithospheric flexure or none at all. The impact of these processes might largely depend upon their region and the relative strength of the plate. In warmer, younger regions along continent margins, sedimentation can significantly reduce plate strength while removal of surface loads via erosion on a weak plate can strongly impact its flexural profile (Lavier and Steckler 1997). Flexure of cratons would be largely unmodified by changes in surface topography due to their high rigidity (e.g. Audet and Burgmann 2011), although mantle effects also impact Te estimations (McKenzie 2010).

McKenzie (2003) investigated continental Te estimates in North America, central Europe, Africa, and Fennoscandia to reveal the importance of dynamically supported topography arising from mantle convection and post-glacial rebound. He concludes that these regions show clear evidence of dynamic support and that post-glacial uplift is causing the gravity field to change with

time. Therefore, none of the regions are currently isostatically compensated, even at long wavelengths. McKenzie argues that coherence studies overestimate the value of Te when dynamically supported topography is modelled with an elastic plate, explaining the high observed Te values in shields. The admittance method however can remove the effect of dynamically supported topography, yielding lower values comparable to rheological studies. McKenzie recognizes that Ts and Te measure fundamentally different properties related to lithospheric strength but asserts that there is no evidence Te should exceed Ts in continental or oceanic regions.

Perez-Gussinye and Watts (2004, 2005) addressed concerns regarding the application of Bouguer coherence. Perez-Gussinye and Watts (2004) approached the problem from a signal processing perspective, utilizing synthetic topography and gravity data for which Te is known. The calculation of both admittance and coherence involves estimation of finite and non-periodic data. Therefore, the wavelength dependence of the admittance and coherence varies with the size of the data window used. They found that when observed coherence and admittance functions are calculated using identical windowing and processing steps, as is usually the case with coherence method, Te estimates yield similar results. Perez-Gussinye and Watts (2004) reformulated theoretical free-air admittance to account for surface and buried loading in a manner consistent with Bouguer coherence developed by Forsyth (1985). Perez-Gussinye and Watts (2005) estimated Te of Europe using both Bouguer coherence and free-air admittance to show that the resulting Te magnitudes are similar and correlate well with geological and other geophysical data (Windley 1992). However, their modelling produces surface and buried loads which are not statistically independent, an assumption required for Forsyth's (1985) coherence method and their revised admittance method. The geologic reality is that loads may very well be correlated statistically and would therefore limit the application of gravitational coherence or the revised admittance model.

Their study also showed that Te exceeds Ts in some regions, an observation which has generated significant debate.

Previous studies (e.g. Jackson and White 1989) have argued that Te and Ts should be comparable in magnitude because of oceanic observations where Te and Ts *are* comparable. However, this is due to the single-layer rheology of oceanic lithosphere. Recent continental studies have constrained Ts to a mostly uniform thickness of 20 km with few exceptions of 40 km in old shields (Maggi et al. 2000b). Maggi et al. (2000a) posits that lithospheric strength is determined by the extent of brittle deformation and Ts should therefore be the same as Te. However, such an assertion implies that lithospheric strength is contained entirely within the crust and that the lithospheric mantle is incapable of maintaining long-term loads. This is in stark disagreement with previous studies which have shown the important of lithospheric mantle in maintaining continental strength (e.g. Sahagian and Holland 1993, Poudjom Djomani et al. 1999, Burov and Watts 2006, Mouthereau et al. 2013).

Watts and Burov (2003) investigated the relationship between effective elastic thickness Te and seismogenic layer thickness Ts. They argue that Te and Te reflect fundamentally different properties of the lithosphere, though both relate to lithospheric strength, hence the historical confusion. Effective elastic thickness reflects the integrated strength of various rheologies (e.g. elastic, ductile, and brittle) on geological time-scales and does not correspond with any subsurface boundary. Seismogenic layer thickness is related strictly to the depth at which anelastic deformation occurs as unstable sliding friction on much shorter time-scales. Thus, Te and Ts reflect different lithospheric properties and should not necessarily be equal. The author of this study is in agreement with Watts and Burov (2003) regarding the interpretation of Te and Ts values.

Perez-Gussinye and Watts (2004) also addressed McKenzie's (2003) conclusion that erosion and sedimentation tend to flatten topography and thus reduces the response of the crust to subsurface loading. They argue that this is inconsistent with a thin plate approximation of flexural isostasy. The removal of a surface mass which produced a subsurface load would induce flexural re-adjustment until the load is compensated at depth. Both the topography and internal load would be reduced such that they reflect a consistent plate rigidity. However, as McKenzie (2003) demonstrated, no internal loading within continental lithosphere exists which produces a strong topographic expression.

The theoretical thin plate model cited by Perez-Gussinye and Watts (2004) does indeed predict flexural readjustment as surface loads migrate through post-tectonic processes. However, this may not be a geologically reasonable assumption, especially in stronger regions. The correlation between Te and thermo-tectonic age of continental lithosphere suggests that plate rigidity resets during major tectonic events through thermal rejuvenation. Consequently, the plate is much weaker at the time of collision or extension and grows progressively stronger as thermal equilibrium is re-established (e.g. Artemieva 2006). Erosion and sedimentation will therefore alter surface loads on a stronger lithosphere than initially produced internal loading and subsequent topographic expression. The greater strength of the lithosphere can "lock in" internal loading while altering the topographic profile through surface processes, resulting in loads which are not expressed in topography. This contradicts a fundamental assumption in Forsyth's (1985) coherence model. Estimations of elastic thickness over region without significant topographic expression of internal loads would thus significantly overestimate the magnitude of Te.

The reduced topography in the Permian Basin and the lateral distance across the region precludes the application of gravitational coherence. Thus, this study applies gravitational

admittance to estimate elastic thickness. The relatively flat landscape does however make it more difficult to evaluate plate strength. The observed admittance function has been modified such that short-wavelength topography has been artificially produced in the wavenumber domain to improve model results. The justification of this approach is addressed in Chapter IV.

CHAPTER IV

METHODOLOGY

4.1 Overview and Dataset Acquisition

A dataset published by the USGS is freely available online and includes 76,550 individual gravimeter readings located in Texas and eastern New Mexico (Bankey 2006). The trimmed dataset utilizes 26,613 gravimeter readings and is presented in Figure 4.2. Data for each gravimeter reading include the observed gravity reading, Bouguer gravity anomaly, free-air gravity anomaly, elevation height, and GPS coordinates. The Bouguer and free-air anomalies are not directly observed readings but rather calculated from the observed gravity after appropriate data reduction procedures are applied (e.g. Lowrie 2004). The complete Bouguer anomaly within the USGS dataset utilized the 1967 gravity reduction formula (e.g. Cordell et al. 1982) and terrain corrections developed by Plouff (1977). These corrections to the observed gravity are adequate for this study and no further data reduction steps to the Bouguer anomaly are necessary.

While software for potential field modelling is commercially available (e.g. Oasis Montaj), the existing programs do not include the ability to model gravitational admittance or calculate effective elastic plate thickness (Te) through inversion. As a result, a large portion of this project was spent developing code to extract Te estimates from gravity and topography data. Four independent scripts for major workflow components were written in Matlab:

1. Hypersurface Creation and Interpolated Signal Extraction
2. Spatial Domain Signal Processing and Transformation to the Wavenumber Domain
3. Calculation of Observed Bouguer Admittance
4. Inversion of Theoretical Curves and Observed Admittance

Each script is expanded upon in the following sub-sections, wherein workflows and functions are described in detail for reproduction purposes. An overview of the conventional admittance methodology is presented in Figure 4.1. A revised methodology which includes the use of the topography regularization parameter (TRP) as part of the observed admittance calculation is presented in Figure 5.1. Material parameters used in the generation of theoretical admittance functions are also presented in Figure 5.1.

Figure 4.1 – Conventional Admittance Methodology

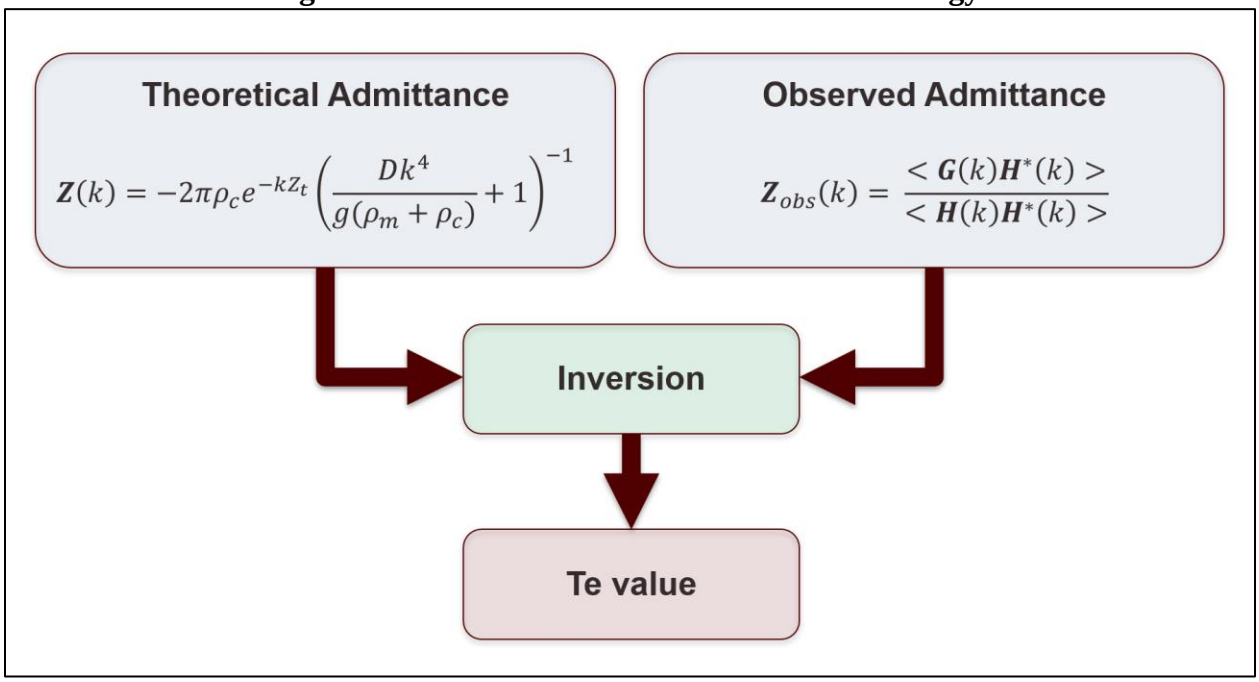

Theoretical admittance functions are calculated according to Equation 3.7. The observed admittance function (without TRP) is calculated by Equation 3.8. A non-linear least-squared inversion is performed to estimate the value of Te along 1-D profile. $\boldsymbol{Z}_{obs}(k)$ is the observed admittance, $\boldsymbol{G}(k)$ is the Fourier transform of the gravity signal g(x), $\boldsymbol{H}(k)$ is the Fourier transform of the topography signal h(x), * denotes the complex conjugate, < > represent an averaging process (see Section 4.4), $\boldsymbol{Z}(k)$ is the theoretical admittance, k is the wavenumber, ρ_m is the density of the mantle, ρ_c is the density of continental crust, γ is the gravitational constant, g is the acceleration due to gravity, Z_t is the mean thickness of the crust, and D is the flexural rigidity constant.

Figure 4.2 – Gravimeter Locations

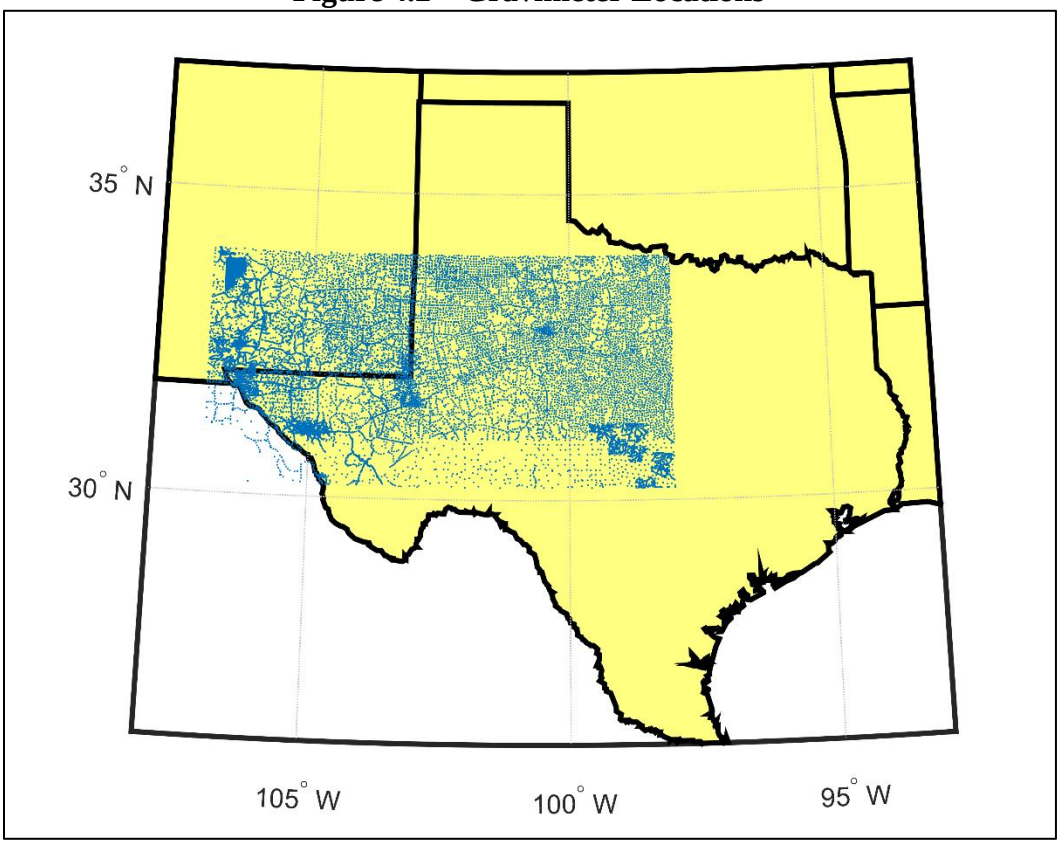

Blue dots represent the 26,613 gravimeter readings used in this study, trimmed from a total of 76,550 gravimeter readings available in USGS dataset. The maximum and minimum data latitudes of the trimmed dataset are 34.0°N and 30.2°N respectively, and the maximum and minimum longitudes are 107°W and 98°W.

4.2 Hypersurface Creation and Interpolated Signal Extraction

The USGS dataset is imported into Matlab and trimmed to the region of study (Figure 4.2). A regular 1000 x 2000 grid is created as the basis for data interpolation. Gravimeter stations are spaced with sufficient density throughout the northern portion of the study region to enable accurate interpolation of the mid-to-long wavelength components of the Bouguer anomaly and topography signals. The larger spacing of gravimeter readings in the southern portion of the study region may bias Te estimations by underestimating the low-to-mid wavelength components of the interpolated signals (see Chapter VI). The process of data interpolation generates a hypersurface

with the Z-values representing the magnitude of a gravity anomaly or elevation. Hypersurfaces are created using the *griddata* function in Matlab (Figures 4.4, 4.5, 4.6, 4.7). Triangulation-based cubic interpolation was chosen for the interpolation algorithm in order to avoid the "spikiness" that is associated with other methods (e.g. nearest neighbor, natural neighbor). Smoother interpolation techniques yield better representations of the signals in the wavenumber domain via the Fourier transform.

Regularly-spaced data distributed along a linear profile on a hypersurface can represent a synthetic 1-D signal. This signal may be regarded as a reasonable proxy to a hypothetical acquisition along a straight transect crossing the study area, although an interpolated signal is not strictly equivalent to a signal acquired through fieldwork. However, utilizing the 1-D signal extraction method from an interpolated hypersurface possesses significant advantages over traditional field acquisition. A continuous, linear acquisition across potentially rugged terrain for thousands of kilometers is a noteworthy investment of time and resources, especially when it only yields one signal. Through interpolation of irregularly-spaced gravimeter readings, multiple signals can be easily "acquired" in any direction, though this method has definite limitations relative to sample density. There is a downward bias of high-wavenumber power in the sparsely sampled USGS dataset which affects effective elastic thickness estimates. This topic is further addressed in Section 4.3.

After the Bouguer anomaly and topography hypersurfaces are generated, the Z-value matrices of the hypersurfaces are sub-divided into East-West oriented 19 zones which are 22 km in width (0.20° in latitude) and on average 846.5 km in length (Figure 4.3). In each zone, 11 individual matrix rows representing synthetic 1-D signals are extracted and saved as arrays every 2 km in a north-south direction (0.02° in latitude) as part of the averaging process developed by

Watts (1978) (see Section 3.2). The signals are east-west oriented at specified latitudes passing over the Delaware Basin, Central Basin Platform, and Midland Basin. Determining Te through numerous east-west oriented zones produces a pseudo 2-D map of Te across the region. The saved signal arrays are processed in the spatial domain in the next script prior to their transformation into the wavenumber domain.

Figure 4.3 – Zonal Division of the Study Region

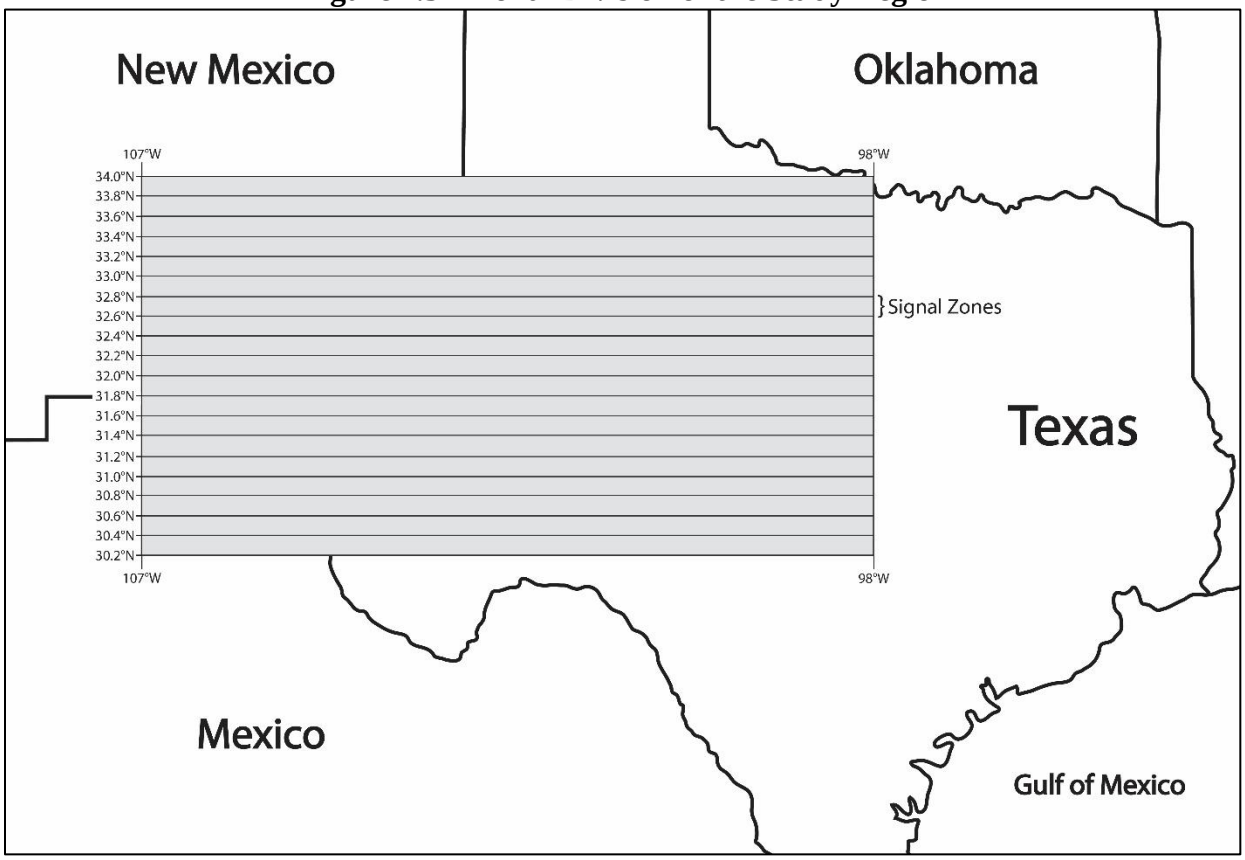

The spatial extent of the trimmed dataset is represented by a grey box and divided into 19 east-west zones with an average zonal length of 846.5 km. The north-south distance for each of the zones is 22 km.

Figure 4.4 – Topography Hypersurface

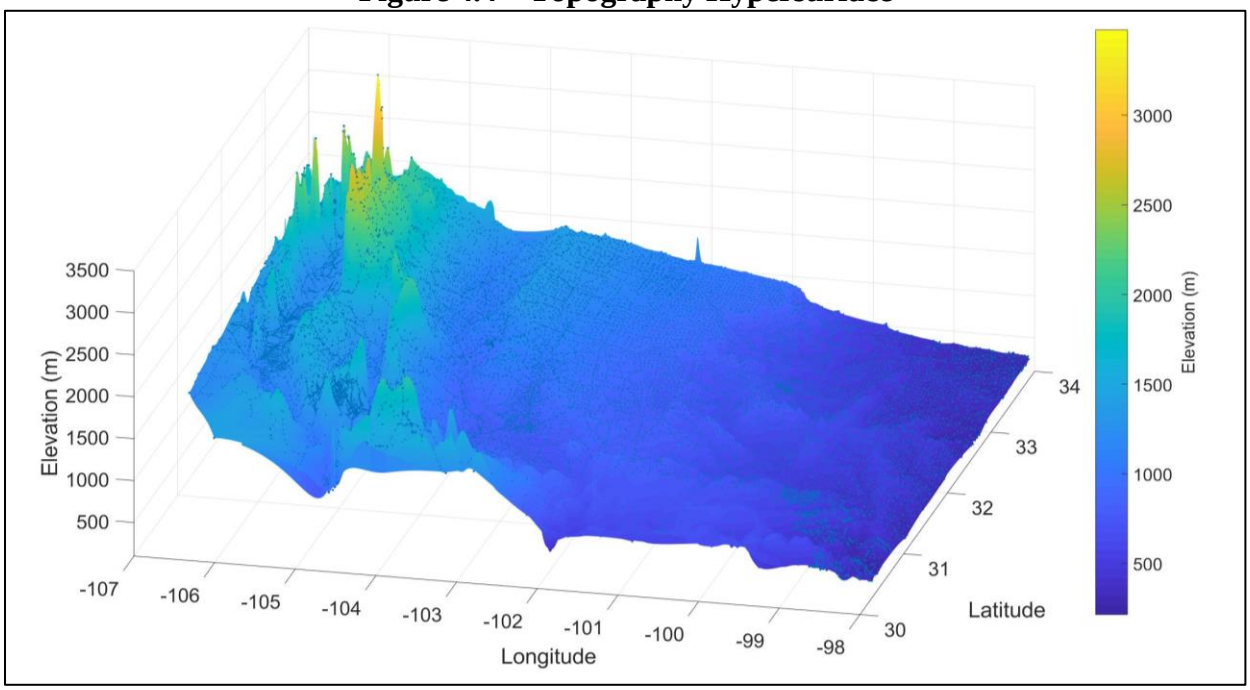

Dots on the surface represent gravimeter locations. The Z-values of hypersurface represent topography and reflect the surface features of the study region.

Figure 4.5 – Bouguer Anomaly Hypersurface

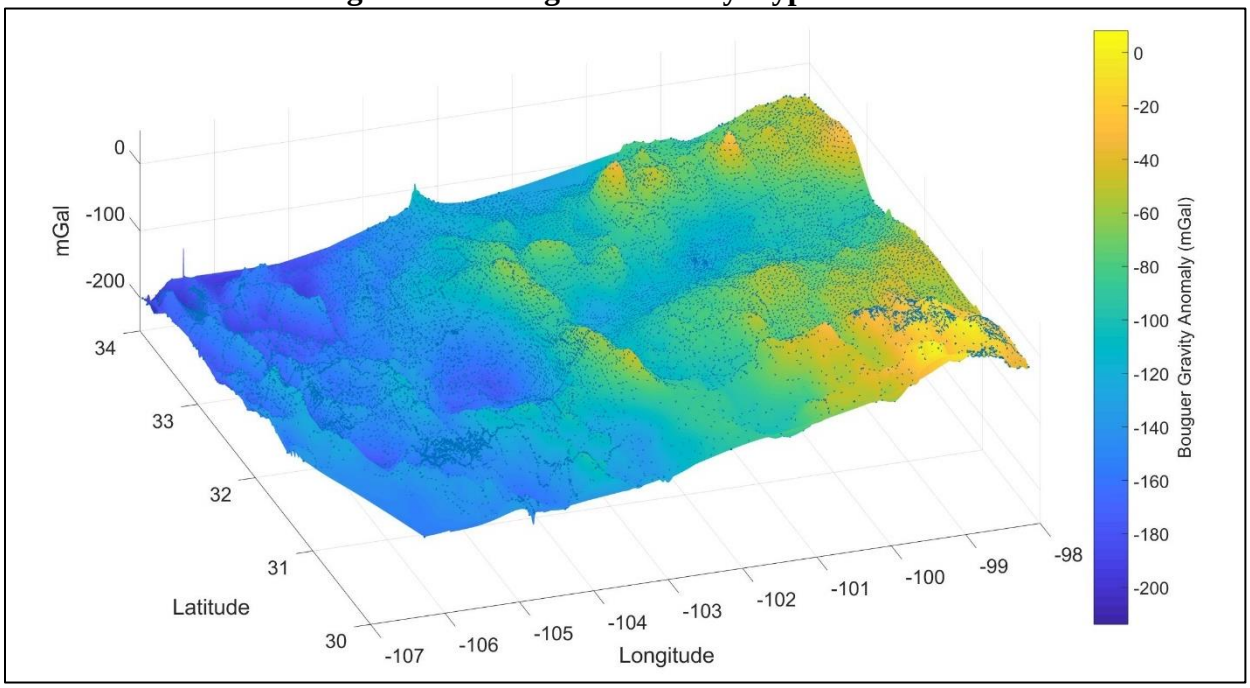

Dots on the surface represent gravimeter locations. The Z-values of hypersurface represent Bouguer anomaly values and reflect the subsurface mass distribution across the study region.

Figure 4.6 – Topography Hypersurface with Extracted Signals

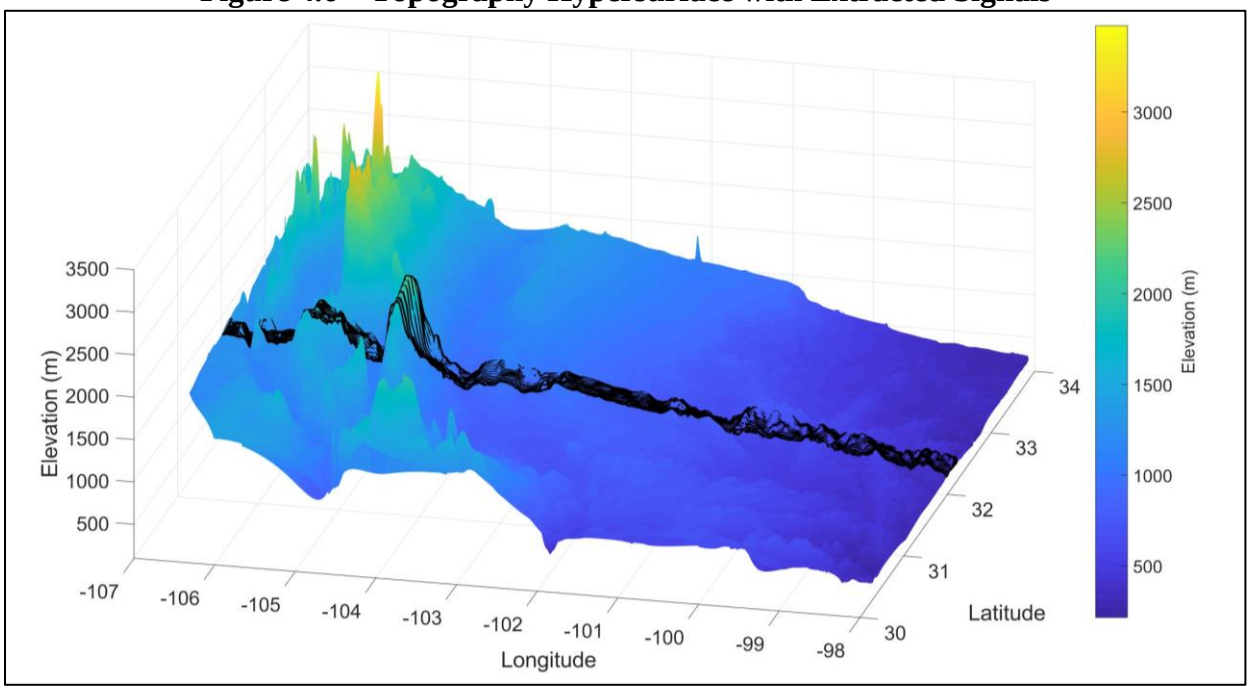

Highlighted in black are 11 topography signals with a spacing of 0.02° (2 km) ranging from 32.0°N to 32.2°N (22 km). These 11 signals represent a single east-west oriented zone.

Figure 4.7 – Bouguer Anomaly Hypersurface with Extracted Signals

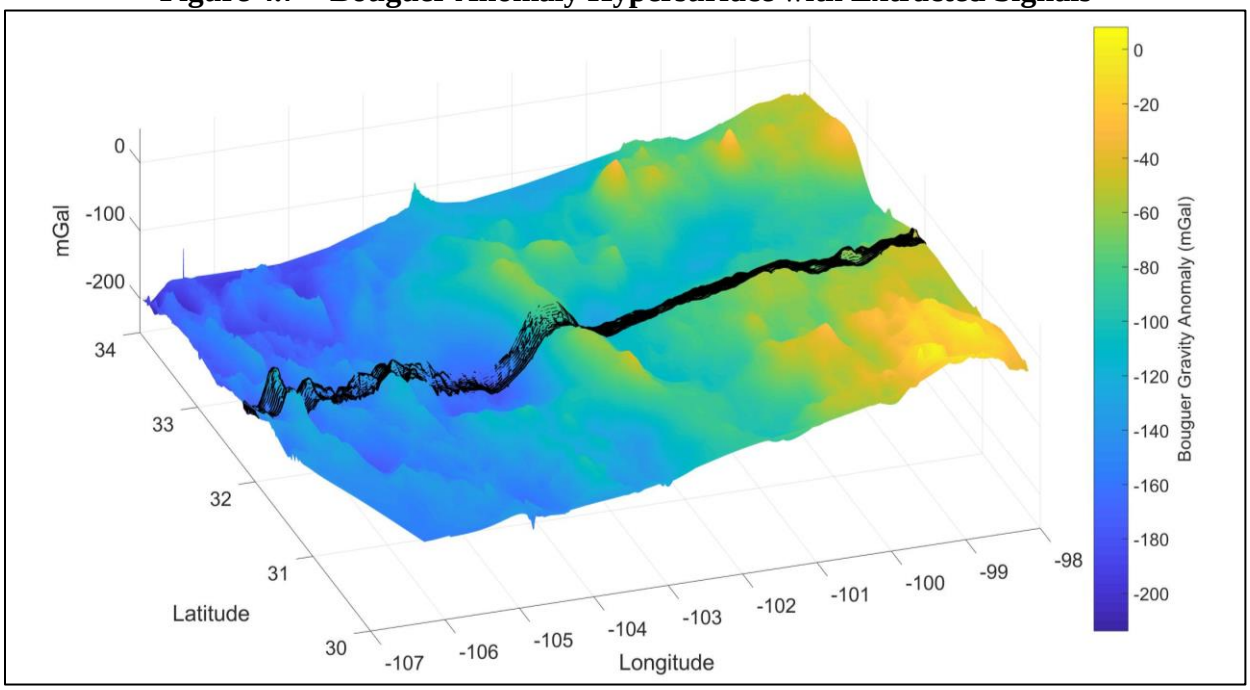

Highlighted in black are 11 topography signals with a spacing of 0.02° (2 km) ranging from 32.0°N to 32.2°N (22 km). These 11 signals represent a single east-west oriented zone.

4.3 Spatial Domain Signal Processing

The purpose of spatial domain filtering of the interpolated signals is to reduce spectral leakage associated with discrete Fourier transforms. Numerous sources such as the Gibbs phenomenon (e.g. Pan 2001), aliasing (e.g. Smith et al. 1996), and windowing (e.g. Simons and Olhede 2012) can cause power from one harmonic to bleed into adjacent harmonics, biasing the frequency spectrum (Brigham 1988, Kirby 2014). Spectral leakage can be minimized by demeaning, detrending, and tapering the signals in the spatial domain prior to their transformation. A low-pass filter can also be applied, though for this project it is not utilized due to the aforementioned issues concerning reduction in power of high wavenumbers caused by the sparse spatial distribution of USGS gravity stations (see Section 4.2).

Spatial domain processing begins with loading of the interpolated signals from the previous script. NaN (not-a-number) values are removed which may exist at signal end-points due to interpolation. Latitude and longitude coordinates of signal endpoints are used to calculate total signal distance in kilometers. A distance vector is then created to plot the interpolated signals in the spatial domain (Figure 4.8). Signals are demeaned and detrended using least squares regression. The residual signals then have a 5% cosine taper applied to both ends of each signal using the *tukeywin* function in Matlab (Figure 4.9). Signals are converted into the wavenumber domain via 1-D fast Fourier transform with the *FFT* function in Matlab (Figure 4.10). Wavenumber signals are then saved and used in the next scripts to calculate observed admittance.

Figure 4.8 – Extracted Interpolated Signals

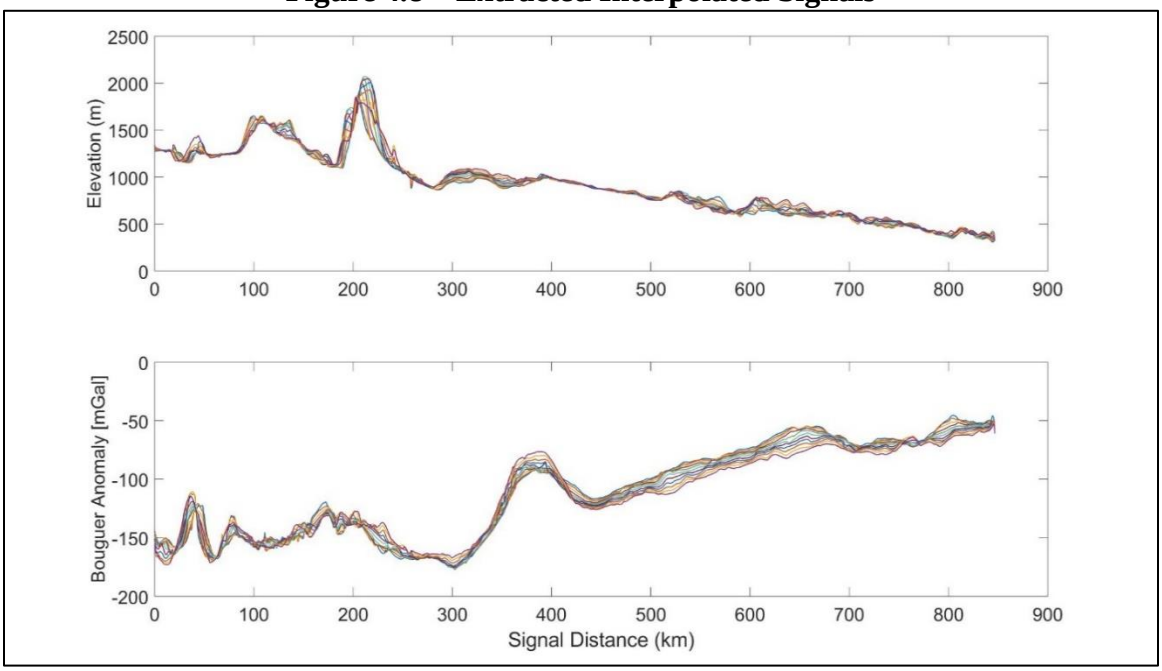

Signals presented are the same 11 signals highlighted in Figure 4.6 & Figure 4.7 ranging from 32.0°N to 32.2°N (22 km) with a spacing of 0.02° (2 km) oriented east-west across the Permian Basin. (Top) Topography signals. (Bottom) Bouguer anomaly signals.

Figure 4.9 – Demeaned and Detrended Signals

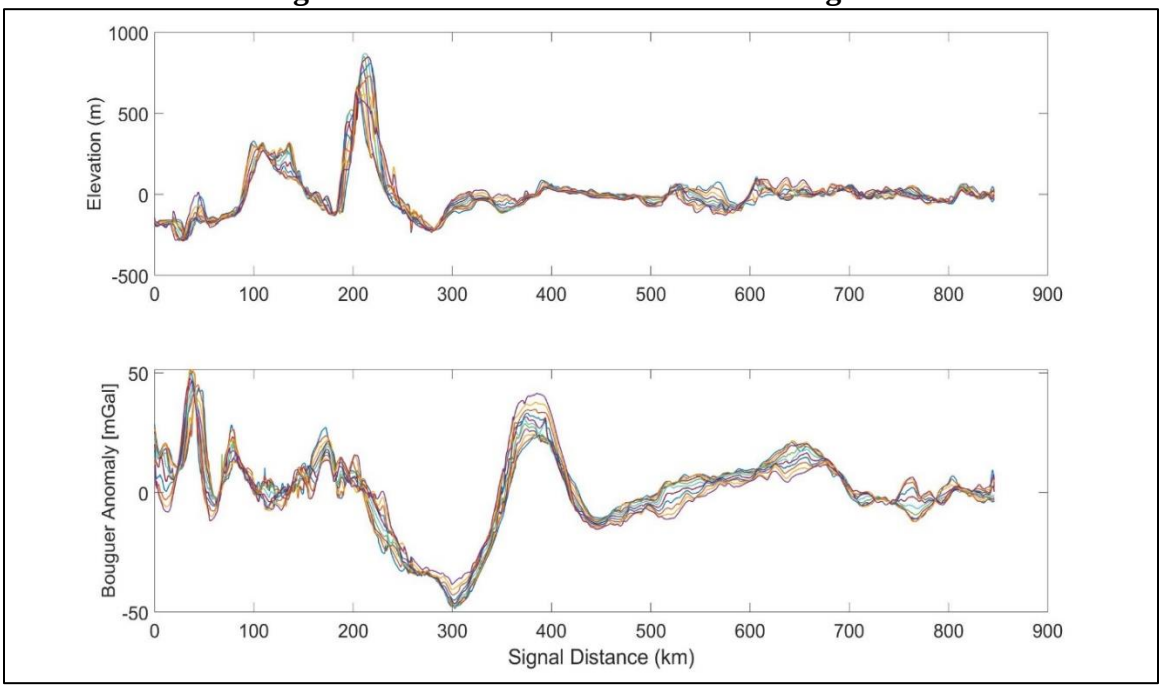

Both the 11 topography signals (Top) and 11 Bouguer anomaly signals (bottom) as shown in Figure 4.8 have had their linear trends remove and set to a mean value of zero. Removal of the linear trend improves representation of the signals in the wavenumber domain via the Fourier transform.

Figure 4.10 – Tapered Signals

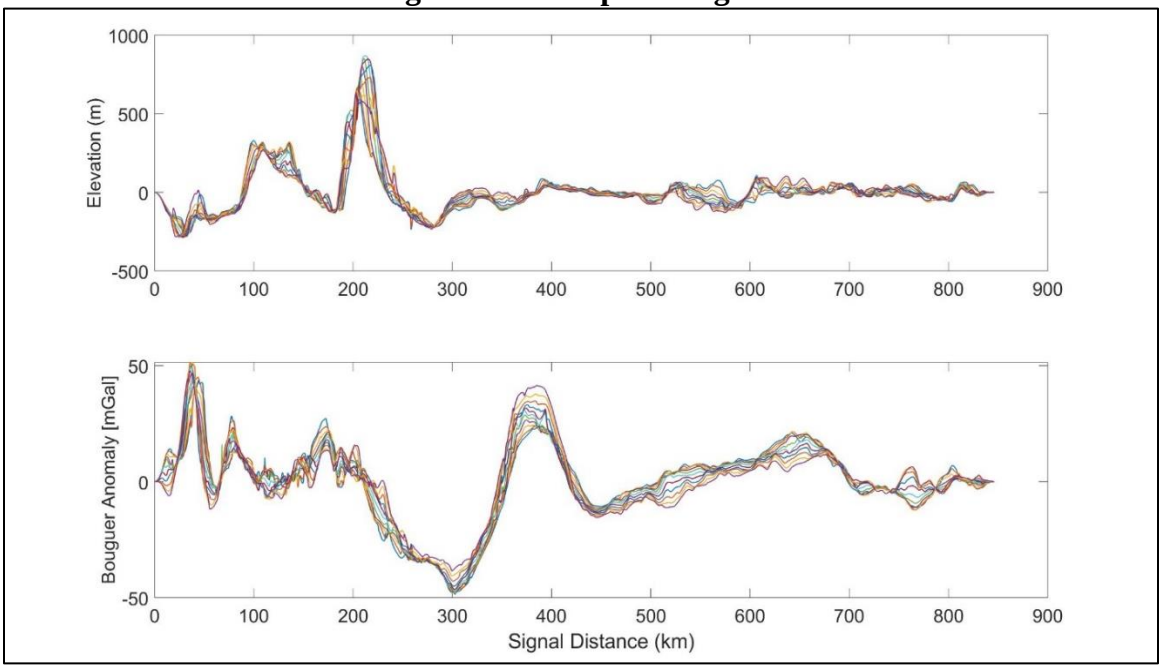

Both the 11 topography signals (Top) and 11 Bouguer anomaly signals (bottom) as shown in Figure 4.9 have been tapered at both ends with a 5% cosine taper via the *tukeywin* function in Matlab.

4.4 Observed Bouguer Admittance

After the Fourier transformed signals are loaded from the previous script, the observed Bouguer admittance function $Z(k)$ would be calculated as defined by Equation 3.4. However, as mentioned in Section 4.2**,** the reduction of high wavenumber power in the topographic signals poses a problem in calculating observed admittance functions. The spacing of gravimeter readings does not allow for topography to be interpolated with the small-scale variations expected of natural terrain, resulting in the reduction of high wavenumber power in topography signals. This in turn biases elastic thickness estimations by reducing the denominator at high wavenumbers and either yields Te values that are much lower than are geologically reasonable or the inversion process fails (see Figure 4.11). A wavenumber parameter is implemented in observed admittance calculations to compensate for this phenomenon (Equation 4.1). This parameter, henceforth called the

topographic regularization parameter or TRP, is a constant (λ) that is added to the denominator of the admittance functions after the multiplication of the averaged topography signal with its complex conjugate. Because this constant is summed with the denominator of the admittance function in the wavenumber domain, it represents a "white noise" contribution to the function, thereby introducing an amplitude correction at all wavenumbers. However, the TRP preferentially biases the high-wavenumbers due to their low amplitudes and effectively produces artificial, small-to-mid scale variations expected of natural topography. As a result, the TRP dampens the falloff of the observed admittance function towards the shape that is theoretically predicted (see Figure 4.12). The TRP magnitude is determined through systematic trial-and-error until the observed admittance curve mostly closely resembles the theoretical functions. Implementation of the TRP improves Te estimations along each zonal profile. The modified observed admittance function incorporating TRP is presented below.

Equation 4.1 – Observed Admittance Function with TRP

$$\boldsymbol{Z}_{obs}^{TRP}(k) = \frac{< \boldsymbol{G}(k)\boldsymbol{H}^{*}(k) >}{< \boldsymbol{H}(k)\boldsymbol{H}^{*}(k) \; + \; \lambda >}$$

Where $\mathbf{G}(k)$ and $\mathbf{H}(k)$ are the gravity and topography signals respectively in the wavenumber domain, $\mathbf{H}^{*}(k)$ is the complex conjugate of $\mathbf{H}(k)$, k is either the 2-D or 1-D wavenumber, and λ is the topographic regularization parameter (TRP). Angle brackets denote an averaging process.

Interpolation is incapable of predicting small variations for the Bouguer anomaly hypersurface as well, though this does not pose a significant issue in calculating Te values. The Bouguer anomaly is expected to have much less power in the high wavenumbers since its calculation removes the gravitational effect of small wavelength near-surface masses above the reference level. Near surface masses are assumed to be uncompensated in terms inducing a flexural

response and thus do not affect the flexural profile of a region. Te estimation should therefore not be affected by reduction of high wavenumber power associated with interpolation of the Bouguer anomaly, and a regularization parameter is not applied to the Bouguer anomaly in the observed admittance calculation.

Two independent smoothing procedures are applied to the observed admittance function prior to inversion. The first step was devised by Watts (1978) whereby spectra of numerous signals across a single geologic feature are combined in the wavenumber domain. The numerator and denominator of the observed admittance function are independently calculated, summed, and then the division process is carried out, collapsing multiple signals into a single function. The averaging of multiple, closely spaced signals across a region captures the gravity and topographic signatures of the regional geology within the latitude limits and helps to prevent Te estimations from becoming biased by a singular geologic features or artifacts inherent in the wavenumber domain representation of the spatial signals. The signals are averaged per the Watts' Method and the TRP is subsequently added into the observed equation.

The second smoothing process involves averaging the observed admittance function over discrete wavenumber bands (e.g. Simons et al. 2000, 2001). Wavenumber band smoothing reduces both the number of data points and the variance of values which in turn improve inversion results. Averaged values for each wavenumber band are plotted at their respective midpoints. Window sizes for the wavenumber band smoothing method are determined by trial and error until the lowest wavenumber value is approximately equal to the theoretical admittance (Table 5.1). The Watts' Method and wavenumber band smoothing method are applied to the observed Bouguer admittance functions for each zone. The observed Bouguer admittance is then saved an array for the inversion process.

A comparison of the observed admittance function without implementation of TRP (Figure 4.11) versus the observed admittance function with implementation of TRP (Figure 4.12) is presented below. Utilization of TRP within the wavenumber calculation of the observed admittance allows for inversion for Te in region of reduced topography.

Figure 4.11 – Observed Admittance Function without TRP

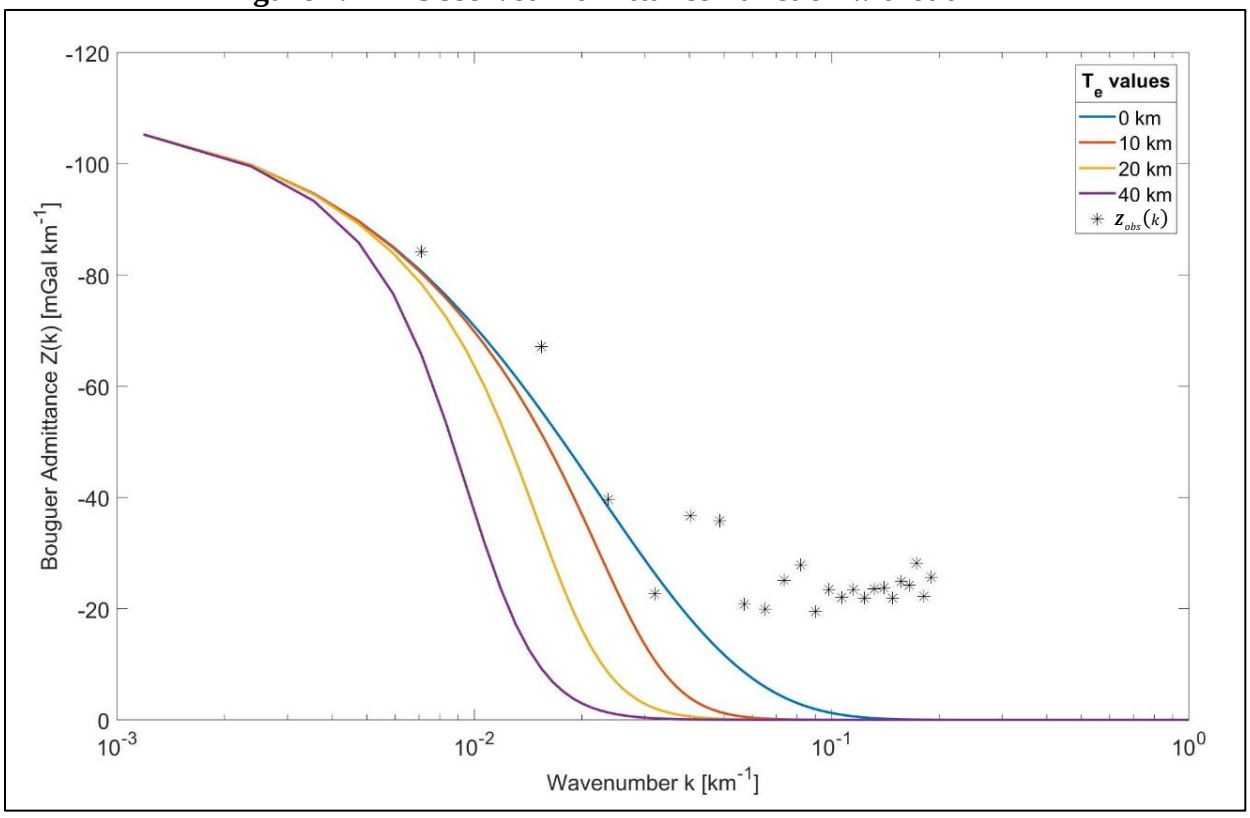

Erosion and interpolation reduce the mid-to-high wavenumber power of the topographic spectrum. As a result, the high wavenumbers of the observed admittance do not approach a value of zero, and inversion for Te either returns an unrealistic value or cannot be achieved through the least-squares method. The observed admittance function presented in this figure has been calculated from the 11 topography signals and 11 Bouguer anomaly signals included in Figure 4.10 and averaged via the Watts' Method and the wavenumber band smoothing method.

Figure 4.12 – Observed Admittance Function with TRP

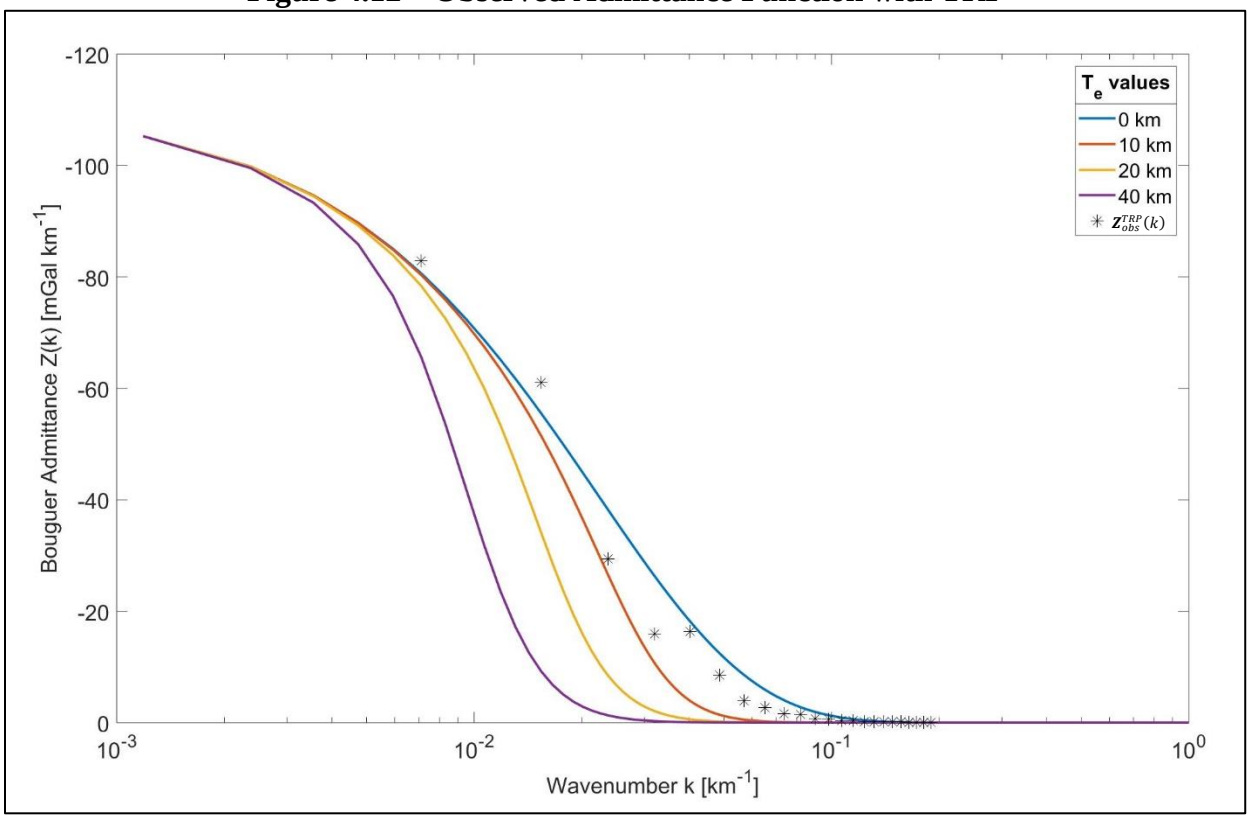

The TRP constant increases the value of the denominator in the observed admittance function and thus dampens the falloff to what is theoretically predicted. Because the largest amplitudes of the topography signals are long-wavelength components, the TRP biases the high wavenumber power without altering the initial shape of the observed admittance at long wavelengths.

4.5 Inversion of Theoretical Admittance and Observed Admittance

The observed Bouguer admittance (Equation 4.1) is loaded and subsequently inverted against the theoretical admittance function (Equation 3.7) using the non-linear least-squares method. Elastic thickness values for the theoretical function range from 1 km to 40 km; only whole number are considered. All other parameters within the theoretical admittance function (Equation 3.7) are held constant throughout the inversion. The values chosen for the theoretical admittance parameters are included in Figure 5.1 The Te value chosen for each zone is the one which minimizes the squared error between the theoretical curves and the observed Bouguer admittance. Inversion results are presented in Chapter V.

CHAPTER V

RESULTS

The parameters used for smoothing and dampening the observed admittance functions are presented in conjunction with their respective zonal Te estimates in Table 5.1. Each table row corresponds with 22 total signals (11 Bouguer anomaly and 11 topography signals) oriented east-west along specific latitude lines from 107°W to 98°W. The corresponding latitude maximum and minimum values define the northern and southern bounds of each east-west oriented zone. The 11 Bouguer anomaly and 11 topography signals cover the same spatial profiles within each zone and are spaced 0.02° in latitude. The Window Size column refers to the number of data values included in the wavenumber band smoothing method. A visual representation of the spatial variations of Te is presented in Figures 5.2, 5.3, and 5.4.

The revised gravitational admittance methodology is presented in Figure 5.1 which includes the implementation of the topographic regularization parameter (TRP) to improve inversion results. Parameter values used in the generation of theoretical admittance curves (Equation 3.7) are included in Figure 5.1. Te estimates for each zone are displayed in Figure 5.2 using a color scale to represent elastic thickness magnitudes. Te values range from 5 km (33.2 – 32.6°N) to 19 km (33.2 – 33.4°N). The average Te value across the region is approximately 10 km. An alternative version of displaying Te estimates is presented in Figure 5.3 to allow for easier interpretation. The Te estimates in Figure 5.3 are represented by a bar graph along the x-axis and a color scale corresponding to the maximum length of each zone's bar.

Te estimates are paired with geologic structures in Figure 5.4. The bar graph has been horizontally scaled and shifted to the right of the study area. Basin uplifts and depocenters are

outlined in bold. Deep crustal features are represented with dashed lines. Not all previously identified geologic features are represented in Figure 5.4, though the major components of the Permian Basin have been included.

Table 5.1 – Inversion Results with Parameter Values

Latitude Minimum	Latitude Maximum	Signal Length (km)	TRP value	Window Size	Te Estimate
34.0	33.8	863	18	16	9
33.8	33.6	861	14	12	8
33.6	33.4	860	10	12	12
33.4	33.2	858	15	14	19
33.2	33.0	856	10	14	6
33.0	32.8	854	10	20	8
32.8	32.6	852	10	14	9
32.6	32.4	851	10	12	5
32.4	32.2	849	12	14	5
32.2	32.0	847	10	14	6
32.0	31.8	845	15	14	8
31.8	31.6	843	15	14	9
31.6	31.4	841	15	14	18
31.4	31.2	839	15	14	12
31.2	31.0	838	10	14	10
31.0	30.8	836	10	14	10
30.8	30.6	834	14	12	13
30.6	30.4	832	15	10	12
30.4	30.2	830	15	12	12

Figure 5.1 – Revised Admittance Methodology

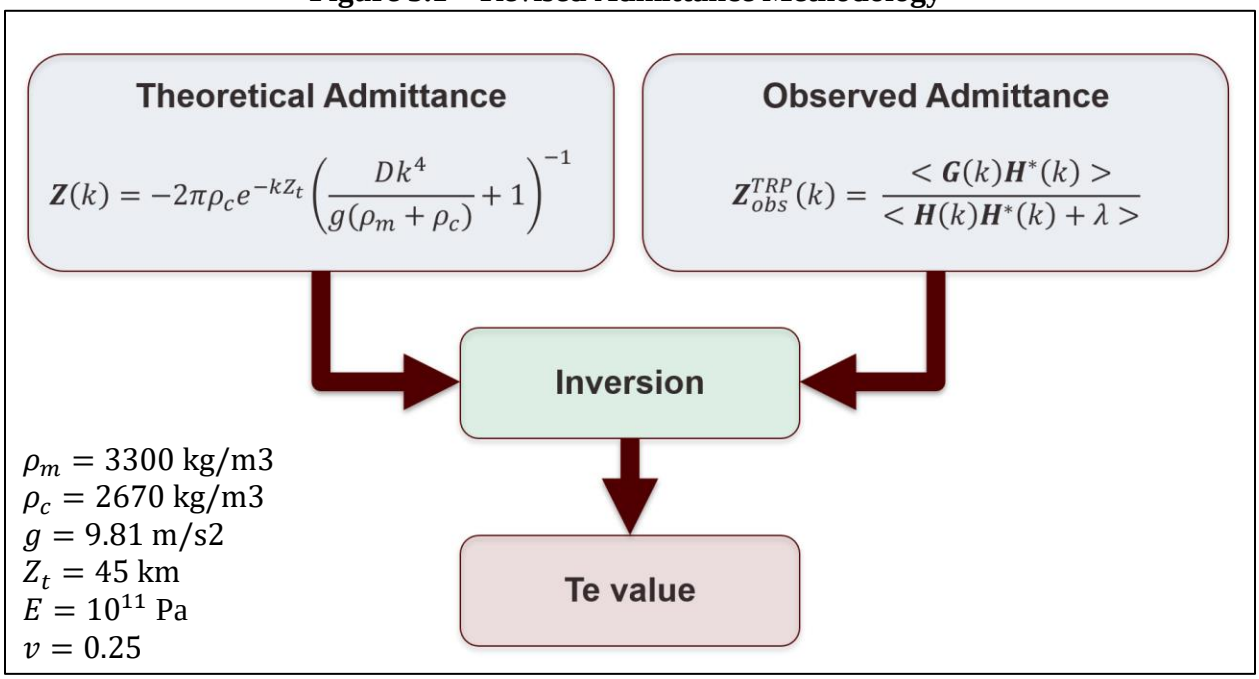

Theoretical admittance functions are calculated according to Equation 3.7. The observed admittance function (with TRP) is calculated by Equation 4.1. A non-linear least-squared inversion is performed to estimate the value of Te along each east-west oriented zone. Material parameters used for the theoretical admittance functions are presented in the bottom left of the figure. $\boldsymbol{Z}_{obs}^{TRP}(k)$ is the revised observed admittance, $\boldsymbol{G}(k)$ is the Fourier transform of the gravity signal g(x), $\boldsymbol{H}(k)$ is the Fourier transform of the topography signal h(x), * denotes the complex conjugate, < > represent an averaging process (see Section 4.4), $\boldsymbol{Z}(k)$ is the theoretical admittance, k is the wavenumber, ρ_m is the density of the mantle, ρ_c is the density of continental crust, γ is the gravitational constant, g is the acceleration due to gravity, Z_t is the mean thickness of the crust, D is the flexural rigidity constant, and λ is the topographic regularization parameter (TRP).

Figure 5.2 – Te Estimates along 19 East-West Oriented Zones

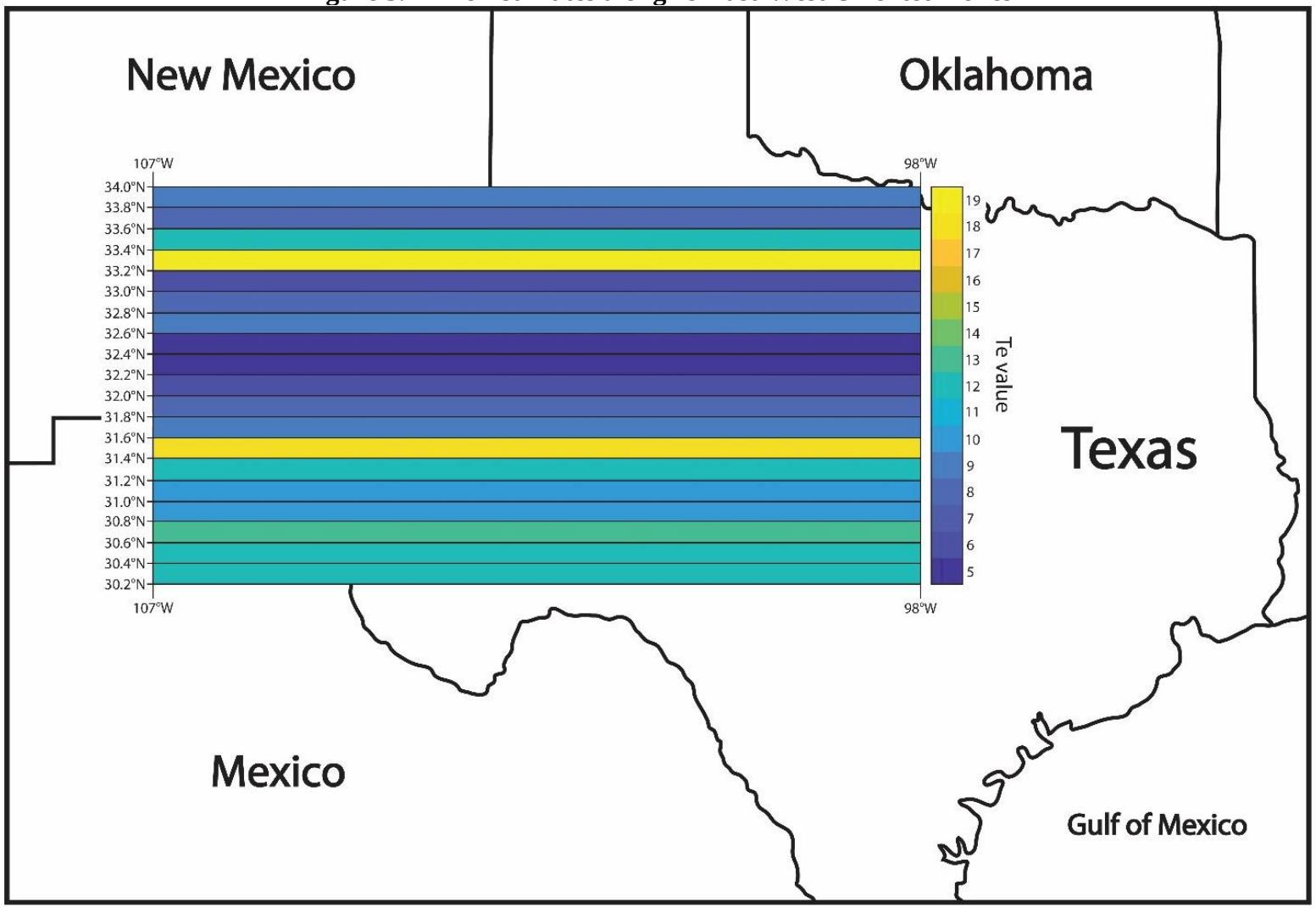

Te values are represented by a color scale. Cooler colors represent lower Te values while warmer colors correspond with higher Te estimates. Values range from 5 km (33.2 – 32.6°N) to 19 km (33.2 – 33.4°N). The average value across the region is approximately 10 km.

Figure 5.3 – Te Estimates along 19 East-West Oriented Zones

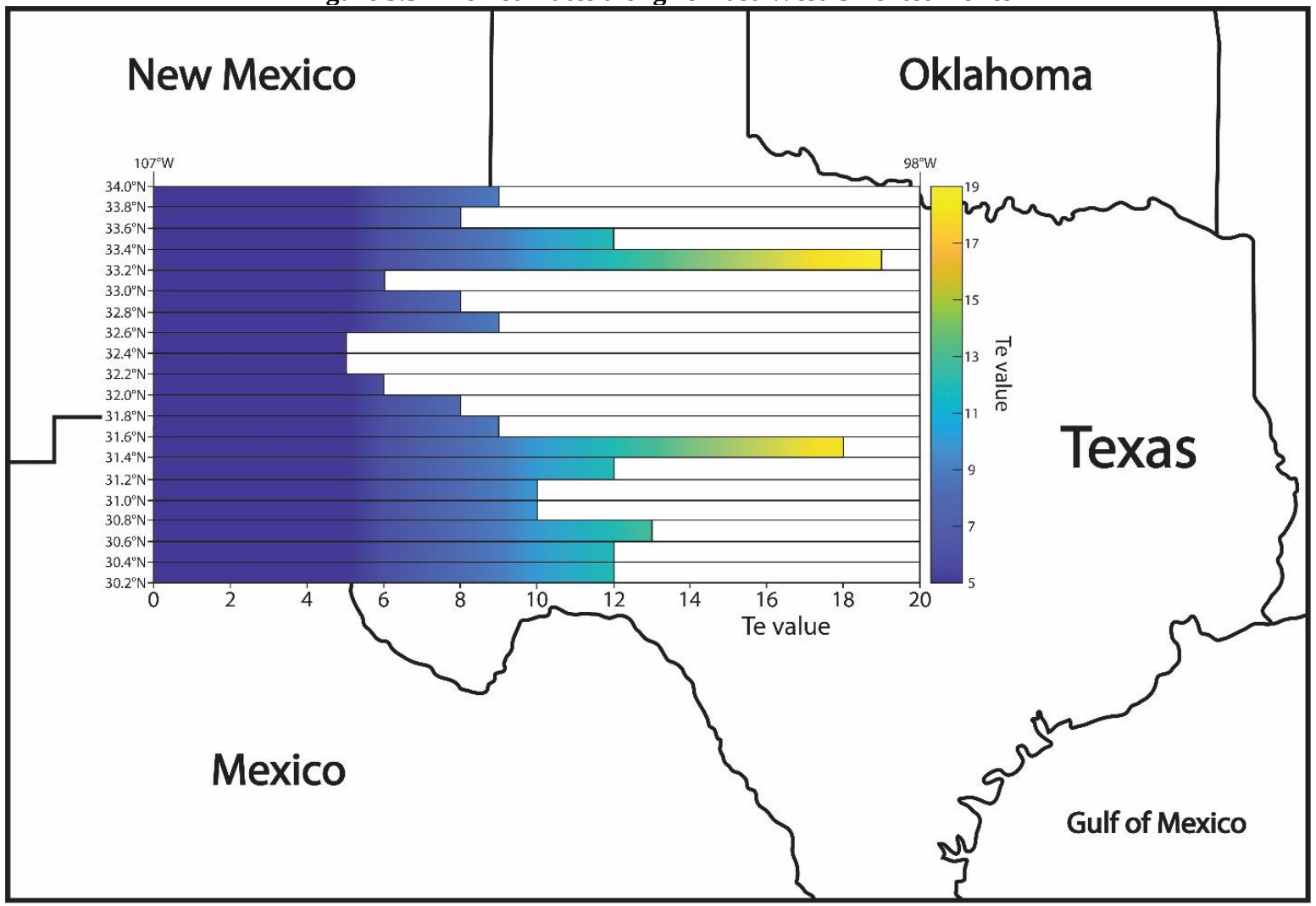

Te values are represented by a bar graph along the x-axis and a color scale corresponding to the maximum length of each zone's bar. A central zone of weakness is identified from 31.6°N to 33.2°N, approximately 176 km in N-S distance. This weak zone is capped by anomalously high Te estimates (19 km in thickness north of the weak zone and 18 km in thickness south of the weak zone).

Figure 5.4 – Te Estimates with Regional Structures of the Permian Basin Region

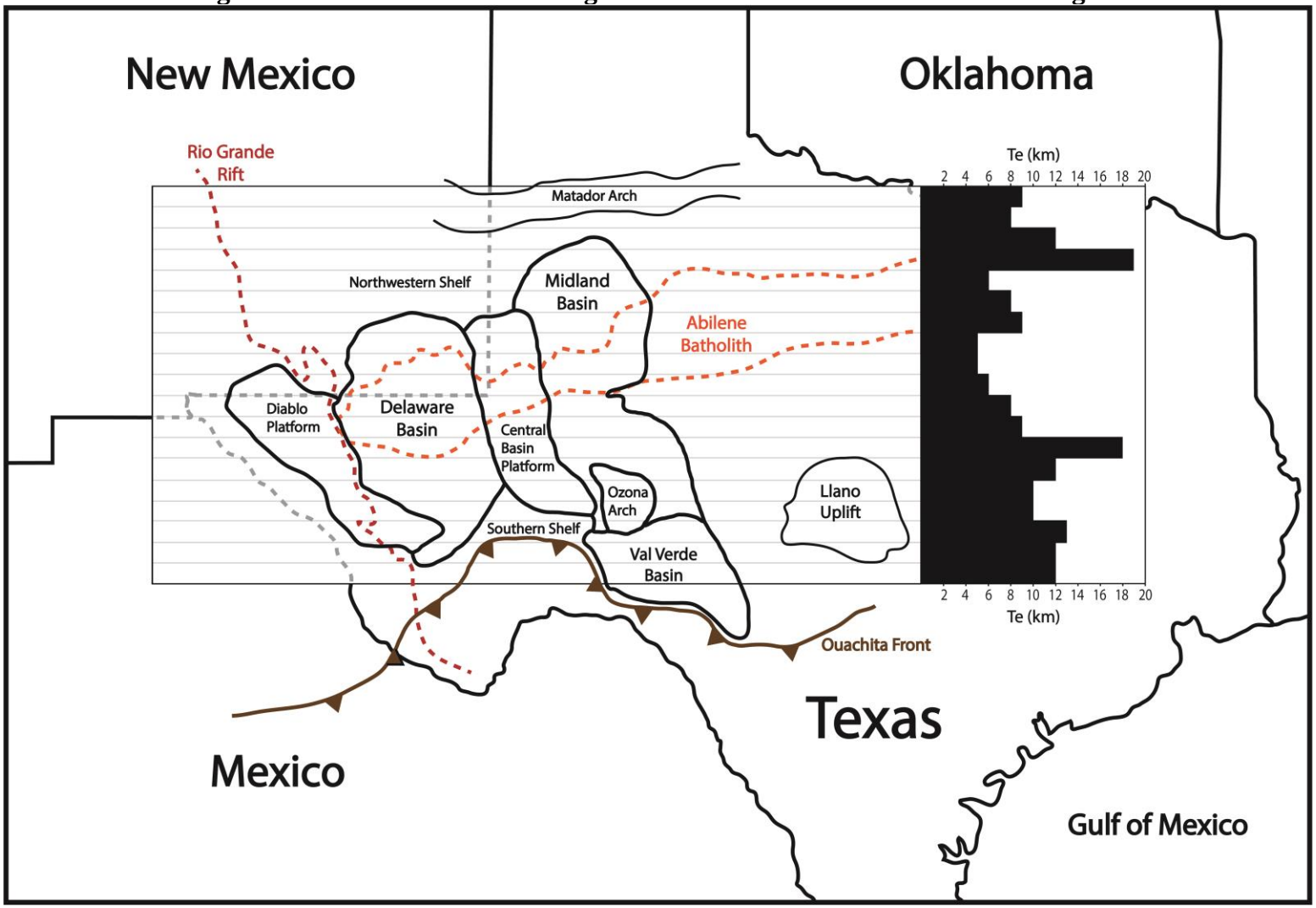

Te values are represented by a bar graph to the right of the study region. Interpreted structures from Adams and Keller (1996) are depicted throughout Texas and New Mexico. Deeper structures are represented with dashed lines. The Abilene Batholith is an interpretation of the Abilene Gravity Minimum.

CHAPTER VI

RESEARCH SUMMARY AND DISCUSSION

Comparison of paleostructures with Te estimates obtained through this study is necessary to validate the revised observed admittance function and implementation of the topographic regularization parameter (TRP). The discussion will be concentrated primarily on the largest geophysical feature in the study area – the Abilene Gravity Minimum (AGM). The AGM is a linear gravity anomaly low approximately 600 km in length that extends throughout the study area and has traditionally been used to mark the location of the Grenville Orogenic Front (e.g. Muehlberger et al. 1967, Reed 1993). The AGM exists almost exclusively within the central zone of low Te values (31.6 – 33.2°N), suggesting that there is a geologic link between this feature and the abnormally weak zone (see Figure 5.4). The origin and composition of the AGM is difficult to constrain due to its depth and lack of well penetration. Work by Adams and Keller (1996) defined more clearly the spatial extent of the AGM by producing a "deep source" gravity map which sharpens the gravity trends of basement and deep crustal features. Adams and Keller (1996) interpret the AGM as a Middle Proterozoic granodioritic continental margin batholith associated with the formation of the South Granite-Rhyolite Province (SGRP). The SGRP refers to the south-central portion of North America formed as a result of Proterozoic magmatism with compositionally similar igneous rocks (Van Schmus et al. 1993).

The AGM marks the southern extent of the SGRP where basement composition transitions from granite-rhyolite to predominantly metasedimentary and gneiss (Adams and Keller 1996). The originating mechanism of the SGRP is unknown, although two main theories have been suggested. The possible mechanisms include an extensional tectonic event (Bickford and Anderson 1993) or

a subduction-related event (Patchett and Ruiz 1989). In either scenario the region would have been weakened by development of structural features and increasing heat flux. Deformational structures preferentially accommodate strain in future tectonic events, thus preserving lithospheric weakness through time (e.g. Poudjom Djomani et al. 1999, Audet and Burgmann 2011, Mouthereau et al. 2013). The presently observed low Te values may be reflecting this inherited lithospheric weakness.

Two anomalously strong zones (32.2 – 32.4°N and 31.4 – 31.6°N) with high Te values (19 km and 18 km respectively) occur on the northern and southern margins of the inner weak zone (31.6 – 33.2°N), outlining the ABM. Though these high Te values are relatively weak in comparison to Archean cratons where Te estimates can exceed 90 km, the containment of the AGM between two strong zones may have geologic significance. The northern margin of the AGM coincides approximately with the northern extent of the Delaware Basin (DB) and Central Basin Platform (CBP) in a region commonly called the Northwestern Shelf (NWS), though the Midland Basin (MB) extends farther north past the AGM. It is important to note that Te values reflect the average lithospheric strength across an east-west zone. Thus, it is not possible to separate the strength variations of multiple features resident in a single zone. The high Te value associated with the northern margin of the AGM and the NWS (33.2 – 33.4°N) may in fact achieve its maximum value in the west. The presence of a weaker zone to the east corresponding to the northern MB may serve to reduce the overall zonal Te estimate. Regardless, the comparatively high Te estimate may reflect strong lithosphere in the western portion of the study region. This increased lithospheric strength may have prevented the DB and CBP from migrating farther north while NW-SE and N-S oriented stresses from the continental collision of Laurentia and Gondwana in the Late Paleozoic deformed the region.

The strong zone along the southern margin of the AGM (31.4 – 31.6°N) coincides with a transition from the deepest part of the DB in the north to a shallower depocenter within the southern DB. This transition can be seen through gravity stripping of sedimentary sections (e.g. Adams and Keller 1996). The AGM exists almost entirely within the deepest portions of the northern DB, though their physical relationship, if any, is not known. Assuming that there is indeed a relationship between Te values and the AGM, meaning that the lithospheric weakness is attributed directly to the AGM, then this suggests that the weakened lithosphere may have increased subsidence within the northern DB. It is also not known whether the weak zone associated with the AGM provided suitable conditions for the batholith emplacement or if the emplacement of the batholith instead weakened the plate. It is possible that both scenarios combined to weaken the region. The lithosphere could have been thermally weakened either through subduction or extension, and the batholith could therefore be preferentially emplaced in the weakest zone. Deep faults may have formed during the emplacement period which would have accommodated strain in subsequent tectonic events. This would result in an inherited weakness of the lithosphere to develop across the AGM. It is also possible that low-density granite comprising the AGM, modelled with 2.64 g/cc by Adams and Keller (1996), is an additional factor in weakening the lithosphere. Further investigation is required before these questions can be answered.

Though the lithosphere across the Permian Basin should be expectedly weak due to the presence of numerous deformational structures, the range of Te estimates (5 – 19 km) produced from this study is low even for a foreland basin. However, comparison of Te estimates produced from this study to results by Yang and Dorobek (1995b) yields similar values. Yang and Dorobek (1995b) performed a 1-D forward model of the flexural response of the lithosphere across the Permian Basin by considering the Central Basin Platform as the load which caused the flexure of

the Delaware and Midland Basins. Their study didn't invert for Te directly but rather estimated flexural rigidity with a range of $10^{21} – 10^{23}$ N·m. Using the range of D from Yang and Dorobek (1995b) and values for Young's modulus (E) and Poisson's ratio (v), Te values can estimated through application of Equation 3.1. The values for E and v in this calculation are the same used in the generation of the theoretical admittance functions (see Figure 5.1). The range of comparable Te values from Yang and Dorobek (1995b) based upon their estimates of flexural rigidity is 4.8 – 22.4 km, which is in close agreement for the range produced from this study (5 – 19 km).

Figure 6.1 displays the range of Te estimates for the Permian Basin region from Yang and Dorobek (1995b), Mouthereau et al. (2013), Audet and Burgmann (2011), and from this study. The global 2-D coherence maps developed by Mouthereau et al. (2013) and Audet and Burgmann (2011) have a wider range of values, 20 – 40 km and 30 – 70 km respectively, with approximately 1-2 Te values each for the Permian Basin region. The resolution of the global Te maps makes it difficult to precisely define the limits of the Permian Basin. Results from this study and from Yang and Dorobek (1995b) display a narrower range of Te values with a lower average value. As noted in Section 3.5, McKenzie and Fairhead (1997) and McKenzie (2003) argue that 2-D coherence studies may be overestimating lithospheric strength. Te results from this study and from Yang and Dorobek (1995b) thus may more accurately represent lithospheric strength across the Permian Basin, especially given that the aforementioned 2-D coherence studies were focused on understanding global trends rather than basin-scale interpretation. The number of Te estimates across the Permian Basin region also increased significantly using a modified version of the 1-D admittance technique with multi-signal zonal averaging over the more conventional 2-D coherence technique. The increased number of Te estimates produced from this study translates to improved spatial resolution of lithospheric strength variations.

Figure 6.1 – Range of Te Estimates in the Permian Basin

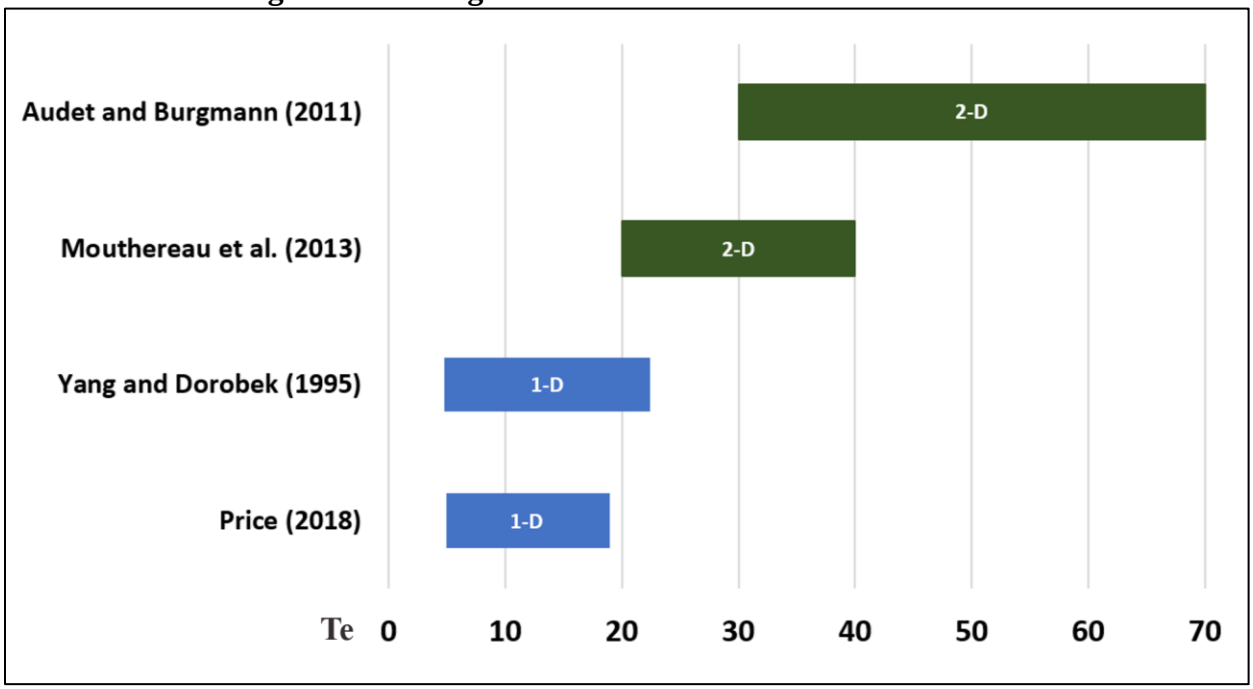

Green bars represent 2-D coherence studies. Blue bars represent 1-D modelling. Work by Audet and Burgmann (2011) and Mouthereau et al. (2013) each produced approximately 1-2 Te values for the Permian Basin region. Yang and Dorobek (1995b) produced a range of flexural rigidity values which were used to estimate a range of Te values. 19 Te values were produced from this study with a range of 5 – 19 km.

Results from this study also show that Te can be accurately estimated in regions which have experienced significant erosion. The implementation of TRP as an additive term in the wavenumber domain representation of the topography signal allows for the stable inversion of Te in regions of reduced topography and sparsely-interpolated data. The magnitude of TRP affects Te estimates which accordingly reduces the geological interpretability of the Te magnitudes. However, the physical meaning of Te has remained obscure in continental studies, showing only strong correlation with thermal and mechanical properties of the lithosphere within oceanic regions (e.g. Watts 2001). Future work could focus on evaluating Te magnitudes with lithospheric properties such as composition, thermal state, and structural features after development of higher resolution Te trend maps.

Given that the estimated Te values and the previously mapped geology of the Permian Basin region are correlated, this study suggests that spectral analysis studies which utilize gravity and topography data to estimate lithospheric strength via the elastic thickness parameter can be used to investigate finer-scaled structure than previously thought. Modern continental studies utilizing 2-D gravitational coherence require a large grid to capture the long wavelengths of flexure in two dimensions. It has been previously recommended that a 1000^2 km grid is adequate for 2-D coherence studies (e.g. Djomani et al. 1995). However, Crosby (2007) demonstrated that stronger regions which should yield a high Te value must have a larger data window than previously considered when utilizing satellite-derived gravity data. The grid size should ideally range from 4000^2 to 8000^2 km depending upon lithospheric strength of the study region. This grid size is far larger than the Permian Basin and thus 2-D gravitational coherence utilizing satellite-derived gravity and topography data (e.g. Audet and Burgmann 2011, Mouthereau et al. 2013) is inadequate for studying lithosphere on a basin-scale.

Weaker regions such as the Permian Basin can utilize smaller data windows since flexure occurs at shorter wavelengths. Returning to 1-D spectral studies collapses the data window to one dimension, further reducing the spatial requirement for Te estimation. The study region for this project is approximately 850 km in length and 420 km in width. Utilizing a zonal discretization combined with multi-signal averaging within each zone, 19 total Te estimates were produced. The utilization of zonal averaging of multiple 1-D signals results in a significant increase in spatial resolution compared to the conventional 2-D coherence method. By increasing the spatial resolution of the Te estimates and correlating with smaller geologic features, studies can begin to constrain the localized effects of geologic process in affecting lithosphere strength. Additionally, if Te can be mapped at higher spatial resolutions and correlated to geologic features, trends in Te

estimates can be used to constrain other lithospheric properties such as composition, thermal conditions, and deep structural features.

The 1-D zonal averaging of multiple E-W oriented signals to estimate Te worked well for this project due to the preferential N-S orientation of the major geological structures within the study region. Future work could focus on estimating Te from zonal averaging performed in other directions and comparing the results to this study. The USGS data used for this project prevented Te from being estimated along N-S oriented signals due to its limited spatial coverage in that direction. Averaging N-S and E-W oriented zones could be attempted in the future with other datasets and in other regions. The aim is to further increase the spatial resolution of Te estimates. A full 360° azimuthal averaging of zones could also be tested to better capture strength variations.

Future work could also focus on implementing TRP more precisely, developing additional methods to boost the high-wavenumber topographical signal at targeted wavelengths with consistent values in regions of erosion and sparsely populated data. Applying a low-pass filter to the Bouguer anomaly signals might accomplish the same result by reducing the power of high wavenumbers in the numerator of the observed admittance calculation. Adding a constant to the denominator via the TRP method or subtracting it from the numerator allows for the observed admittance function to dampen toward the theoretical curves. The latter method would remove the effects of near-surface mass anomalies below the reference level used for the Bouguer anomaly reduction technique (usually given to be sea level). These near-surface features can be considered "geologic noise" that is not related to flexure and their subtraction from the gravity anomaly signals may therefore be appropriate.

The effects of noise have long negatively impacted admittance and coherence studies in estimating continental Te values. Implementation of the TRP aims to mitigate the effects of noise

by artificially boosting the wavenumber spectrum of topographic signals. It has been found that observed admittance curves improve drastically, allowing for Te to be reliably estimated in heavily eroded regions. Correlation between the known geology of the Permian Basin and Te estimates from this study are promising, opening up possibilities to further increase the spatial resolution of Te estimates for regional flexural studies.

REFERENCES

Adams, D. and R. Keller (1996). Precambrian Basement Geology of the Permian Basin Region of West Texas and Eastern New Mexico: A Geophysical Perspective. v. 80(3): 410-431.

Adams, J. E. (1965). Stratigraphic-Tectonic Development of Delaware Basin. *AAPG Bulletin,* v. 49(11): 2140-2148.

Armstrong, G. D. and A. B. Watts (2001). Spatial variations in Te in the southern Appalachians, eastern United States. *Geophysical Journal International,* v. 106(B10): 22009–22026.

Artemieva, I. M. (2006). Global 1°×1° thermal model TC1 for the continental lithosphere: Implications for lithosphere secular evolution. *Tectonophysics,* v. 416(1): 245-277.

Audet, P. (2013). Toward mapping the effective elastic thickness of planetary lithospheres from a spherical wavelet analysis of gravity and topography. *Physics of the Earth and Planetary Interiors,* v. 226: 48-82.

Audet, P. and R. Burgmann (2011). Dominant role of tectonic inheritance in supercontinent cycles. *Nature Geoscience,* v. 4: 184.

Bankey, V. (2006). Texas Gravity and Magnetic Maps Data: A Website for Distribution of Data. US Department of Interior: US Geologic Survey.

Banks, R. J., S. C. Francis, et al. (2001). Effects of loads in the upper crust on estimates of the elastic thickness of the lithosphere. *Geophysical Journal International,* v. 145(1): 291-299.

Banks, R. J., R. L. Parker, et al. (1977). Isostatic compensation on a continental scale: local versus regional mechanisms. *Geophysical Journal of the Royal Astronomical Society,* v. 51(2): 431-452.

Beaumont, C. (1981). Foreland basins. *Geophysical Journal International,* v. 65(2): 291-329.

Belleguic, V., P. Lognonné, et al. (2005). Constraints on the Martian lithosphere from gravity and topography data. *Journal of Geophysical Research: Planets,* v. 110(E11).

Beuthe, M. (2008). Thin elastic shells with variable thickness for lithospheric flexure of one-plate planets. *Geophysical Journal International,* v. 172(2): 817-841.

Bickford, M. E. and J. L. Anderson (1993). Middle Proterozoic Magmatism. Precambrian conterminous U.S. J. C. Reed et al. Boulder. *Geological Society of America, The Geology of North America*. v. C-2: 281–292.

Brigham, E. O. (1988). The Fast Fourier Transform and its Applications. Englewood Cliffs, NJ. Prentice Hall.

Burov, E. and A. Watts (2006). The long-term strength of continental lithosphere: "Jelly Sandwich" or "Crème Brûlée"?

Burov, E. B. (2011). Rheology and strength of the lithosphere. *Marine and Petroleum Geology,* v. 28(8): 1402-1443.

Burov, E. B. and M. Diament (1992). Flexure of the continental lithosphere with multilayered rheology. *Geophysical Journal International,* v. 109(2): 449-468.

Burov, E. B. and M. Diament (1995). The effective elastic thickness (Te) of continental lithosphere: What does it really mean? *Journal of Geophysical Research: Solid Earth,* v. 100(B3): 3905-3927.

Byerlee, J. D. D. (1978). Friction of Rocks. *Pure and Applied Geophysics,* v. 116: 615-626.

Caldwell, J. G. and D. L. Turcotte (1979). Dependence of the thickness of the elastic oceanic lithosphere on age. *Journal of Geophysical Research: Solid Earth,* v. 84(B13): 7572-7576.

Calmant, S., J. Francheteau, et al. (1990). Elastic Layer Thickening with Age of the Oceanic Lithosphere: A Tool for Prediction of the Age of Volcanoes or Oceanic Crust. *Geophysical Journal International,* v. 100(1): 59-67.

Coakley, B. J. and A. B. Watts (1991). Tectonic controls on the development of unconformities: The North Slope, Alaska. *Tectonics,* v. 10(1): 101-130.

Cordell, L., G. R. Keller, et al. (1982). Bouguer gravity map of the Rio Grande Rift, Colorado, New Mexico, and Texas. U.S. Geological Survey Geophysical Investigations Series. Map GP-949.

Crosby, A. G. (2007). An assessment of the accuracy of admittance and coherence estimates using synthetic data. *Geophysical Journal International,* v. 171(1): 25-54.

De Bremaecker, J. C. (1977). Is the oceanic lithosphere elastic or viscous? *Journal of Geophysical Research,* v. 82(14): 2001-2004.

De Rito, R. F., F. A. Cozzarelli, et al. (1986). A forward approach to the problem of nonlinear viscoelasticity and the thickness of the mechanical lithosphere. *Journal of Geophysical Research: Solid Earth,* v. 91(B8): 8295-8313.

Denison, R. E. and A. E. Hetherington (1969). Basement rocks in far west Texas and south-central New Mexico. Border stratigraphy symposium. F. E. Kottlowski and D. V. Lemone. Socorro. New Mexico Bureau of Mines Circular. 104: 1-16.

Djomani, Y. H. P., J. M. Nnange, et al. (1995). Effective elastic thickness and crustal thickness variations in west central Africa inferred from gravity data. *Journal of Geophysical Research: Solid Earth,* v. 100(B11): 22047-22070.

Engle, M. A., F. R. Reyes, et al. (2016). Geochemistry of formation waters from the Wolfcamp and “Cline” shales: Insights into brine origin, reservoir connectivity, and fluid flow in the Permian Basin, USA. *Chemical Geology*, v. 425: 76-92.

Flawn, P. T. (1956). Basement Rocks of Texas and Southeastern New Mexico. Austin. Bureau of Economic Geology, University of Texas.

Flemings, P. B. and T. E. Jordan (1990). Stratigraphic modeling of foreland basins: Interpreting thrust deformation and lithosphere rheology. *Geology*, v. 18(5): 430-434.

Forsyth, D. W. (1985). Subsurface loading and estimates of the flexural rigidity of continental lithosphere. *Journal of Geophysical Research: Solid Earth*, v. 90(B14): 12623-12632.

Galley, J. E. (1958). Oil and Geology in the Permian Basin of Texas and New Mexico. Habitat of Oil. L. G. Weeks. American Association of Petroleum Geologists.

Gardiner, W. B. (1990a). Fault fabric and structural provinces of the Central Basin Platform: a model for strike-slip movement. Permian Basin Oil and Gas Fields: Innovative Ideas in

Exploration and Development. J. E. F. a. R. C. Price. *West Texas Geological Society*. v. 90-87: 15-27

Gardiner, W. B. (1990b). Structral subprovinces of the Central Basin Platform, west Texas. Strike-slip bounded crustal blocks. *AAPG Bulletin*, v. 74: 659.

Goetze, C. and B. Evans (1979). Stress and temperature in the bending lithosphere as constrained by experimental rock mechanics. *Geophysical Journal of the Royal Astronomical Society*, v. 59(3): 463-478.

Hartley, R. (1995). Isostasy of Africa: Implications for the Thermo-Mechanical Behavior of the Continental Lithosphere. Oxford University. PhD.

Henry, C. D. and J. G. Price (1985). Summary of the tectonic development of Trans-Pecos Texas. Bureau of Economic Geology. The University of Texas at Austin.

Henry, C. D. and J. G. Price (1986). Early Basin and Range development in Trans-Pecos Texas and adjacent Chihuahua: Magmatism and orientation, timing, and style of extension. *Journal of Geophysical Research,* v. 91: 6213-6224.

Henry, C. D., J. G. Price, et al. (1991). Mid-Cenozoic stress evolution and magmatism in the southern Cordillera, Texas and Mexico: Transition from continental arc to intraplate extension. *Journal of Geophysical Research,* v. 96: 13545-13560.

Hills, J. M. (1963). Late Paleozoic tectonics and mountain ranges, western Texas to southern Colorado. *AAPG Bulletin,* v. 47(9): 1709-1725.

Hills, J. M. (1970). Paleozoic structural directions in southern Permian Basin, West Texas and southeastern new Mexico. *AAPG Bulletin,* v. 54: 1809-1827.

Hills, J. M. (1984). Sedimentation, Tectonism, and Hydrocarbon Generation in Delaware Basin, West Texas and Southeastern New Mexico. *AAPG Bulletin,* v. 68(3): 250-267.

Hills, J. M. (1985). Structural Evolution of the Permian Basin of West Texas and New Mexico. Structure and Tectonics of Trans-Pecos Texas. P. W. Dickerson and W. M. Muehlberger. Midland, Texas. West Texas Geological Society.

Hoak, T., K. Sundberg, et al. (1998). Overview of the Structural Geology and Tectonics of the Central Basin Platform, Delaware Basin, and Midland Basin, West Texas and New Mexico. Germantown, Maryland.

Horak, R. L. (1985). Tectonic and Hydrocarbon Maturation History in the Permian Basin. *Oil and Gas Journal,* v. 83(21): 124-129.

Jackson, J. A. and N. J. White (1989). Normal faulting in the upper continental crust: observations from regions of active extension. *Journal of Structural Geology,* v. 11(1): 15-36.

Jordan, T. H. (1978). Composition and development of the continental tectosphere. *Nature,* v. 274: 544.

Karner, G. D. (1982). Spectral representation of isosatic models. *BMR Journal of Australian Geology and Geophysics,* v. 7(1): 55-62.

Karner, G. D. and A. B. Watts (1982). On isostasy at Atlantic-type continental margins. *Journal of Geophysical Research: Solid Earth,* v. 87(B4): 2923-2948.

Karner, G. D. and A. B. Watts (1983). Gravity anomalies and flexure of the lithosphere at mountain ranges. *Journal of Geophysical Research: Solid Earth,* v. 88(B12): 10449-10477.

Keller, R., J. M Hills, et al. (1980). A regional geological and geophysical study of the Delaware basin, New Mexico and west Texas. New Mexico Geological Society Guidebook. 31st Field Conference. Trans-Pecos Region. University of Texas at El Paso.

Kirby, J. and C. J. Swain (2011). Improving the spatial resolution of effective elastic thickness estimation with the fan wavelet transform. *Computers & Geosciences,* v. 37(9): 1345-1354.

Kirby, J. F. (2014). Estimation of the effective elastic thickness of the lithosphere using inverse spectral methods: The state of the art. *Tectonophysics,* v. 631(C): 87-116.

Kirby, J. F. and C. J. Swain (2009). A reassessment of spectral Te estimation in continental interiors: The case of North America. *Journal of Geophysical Research: Solid Earth,* v. 114(B8).

Lago, B. and A. Cazenave (1981). State of stress in the oceanic lithosphere in response to loading. *Geophysical Journal International,* v. 64(3): 785-799.

Lambeck, K. and S. M. Nakiboglu (1981). Seamount loading and stress in the ocean lithosphere: 2. Viscoelastic and elastic-viscoelastic models. *Journal of Geophysical Research: Solid Earth,* v. 86(B8): 6961-6984.

Lavier, L. L. and M. S. Steckler (1997). The effect of sedimentary cover on the flexural strength of continental lithosphere. *Nature,* v. 392: 843.

Lewis, B. T. R. and L. M. Dorman (1970). Experimental isostasy: 2. An isostatic model for the U.S.A. derived from gravity and topographic data. *Journal of Geophysical Research,* v. 75(17): 3367-3386.

Love, A. E. H. (1906). A treatise on the mathematical theory of elasticity. Cambridge. University Press.

Lowrie, W. (2004). Fundamentals of Geophysics. Cambridge University Press.

Lowry, A. R. and R. B. Smith (1995). Strength and rheology of the western U.S. Cordillera. *Journal of Geophysical Research: Solid Earth,* v. 100(B9): 17947-17963.

Lowry, A. R. and S. Zhong (2003). Surface versus internal loading of the Tharsis rise, Mars. *Journal of Geophysical Research: Planets,* v. 108(E9).

Maggi, A., J. A. Jackson, et al. (2000a). Earthquake focal depths, effective elastic thickness, and the strength of the continental lithosphere. *Geology,* v. 28: 495-498.

Maggi, A., J. A. Jackson, et al. (2000b). A re-assessment of focal depth distributions in southern Iran, the Tien Shan and northern India: do earthquakes really occur in the continental mantle? *Geophysical Journal International,* v. 143(3): 629-661.

McKenzie, D. (2003). Estimating Te in the presence of internal loads. *Journal of Geophysical Research: Solid Earth,* v. 108(B9): 2348.

McKenzie, D. (2010). The influence of dynamically supported topography on estimates of Te. *Earth and Planetary Science Letters,* v. 295(1-2): 127-138.

McKenzie, D. and C. Bowin (1976). The relationship between bathymetry and gravity in the Atlantic Ocean. *Journal of Geophysical Research,* v. 81(11): 1903-1915.

McKenzie, D. and D. Fairhead (1997). Estimates of the effective elastic thickness of the continental lithosphere from Bouguer and free air gravity anomalies. *Journal of Geophysical Research: Solid Earth,* v. 102(B12): 27523-27552.

McNutt, M. K. (1983). Influence of plate subduction on isostatic compensation in northern California. *Tectonics,* v. 2(4): 399-415.

McNutt, M. K., M. Diament, et al. (1988). Variations of elastic plate thickness at continental thrust belts. *Journal of Geophysical Research: Solid Earth,* v. 93(B8): 8825-8838.

McNutt, M. K. and R. L. Parker (1978). Isostasy in Australia and the Evolution of the Compensation Mechanism. *Science,* v. 199(4330): 773-775.

Mouthereau, F., A. B. Watts, et al. (2013). Structure of orogenic belts controlled by lithosphere age. *Nature Geoscience,* v. 6: 785.

Muehlberger, W. R., R. C. Belcher, et al. (1978). Quaternary faulting in Trans-Pecos Texas. *Geology,* v. 6: 337-340.

Muehlberger, W. R., R. E. Denison, et al. (1967). Basement rocks in continental interior of United States. *AAPG Bulletin,* v. 51: 2351-2380.

Munk, W. H. and D. E. Cartwright (1966). Tidal Spectroscopy and Prediction. *Philosophical Transactions of the Royal Society of London,* v. 259(1105): 533-581.

Pan, C. (2001). Gibbs phenomenon removal and digital filtering directly through the fast Fourier transform. *IEEE Transactions on Signal Processing,* v. 49: 444-448.

Patchett, P. J. and J. Ruiz (1989). Nd isotopes and the origin of Grenville-age rocks in Texas: implications for Proterozoic evolution of the United States Mid-Continent region. *Journal of Geology,* v. 97: 685-695.

Pérez-Gussinyé, M., R. Lowry Anthony, et al. (2004). On the recovery of effective elastic thickness using spectral methods: Examples from synthetic data and from the Fennoscandian Shield. *Journal of Geophysical Research: Solid Earth,* v. 109(B10): B10409.

Pérez-Gussinyé, M., C. J. Swain, et al. (2009). Spatial variations of the effective elastic thickness, Te, using multitaper spectral estimation and wavelet methods: examples from synthetic data and application to South America. *Geochemistry, Geophysics, Geosystems,* v. 10(4): Q04005.

Pérez-Gussinyé, M. and A. B. Watts (2005). The long-term strength of Europe and its implications for plate-forming processes. *Nature,* v. 436: 381.

Pindell, J. L. (1985). Alleghenian reconstruction and subsequent evolution of the Gulf of Mexico, Bahamas, and Proto-Caribbean. *Tectonics,* v. 4(1): 1-39.

Plouff, D. (1977). Preliminary documentation for a FORTRAN program to compute gravity terrain corrections based on topography digitized on a geographic grid. U.S. Geological Survey Open-File Report. 77-535: 45.

Poudjom Djomani, Y. H., J. Derek Fairhead, et al. (1999). The flexural rigidity of Fennoscandia: Reflection of the tectonothermal age of the lithospheric mantle. *Earth and Planetary Science Letters,* v. 174: 139-154.

Reed, J. C. (1993). Map of the Precambrian rocks of the conterminous United States. The Geology of North America: Precambrian contermionous U.S. J. C. Reed et al. Boulder. Geologic Society of America. C-2.

Sahagian, D. L. and S. M. Holland (1993). On the thermo-mechanical evolution of continental lithosphere. *Journal of Geophysical Research: Solid Earth,* v. 98(B5): 8261-8274.

Simons, F. and S. C. Olhede (2012). Maximum-likelihood estimation of lithospheric flexural rigidity, initial-loading fraction, and load correlation, under isotropy. *Geophysical Journal International,* v. 193(3): 1300-1342.

Simons, F. J., M. T. Zuber, et al. (2000). Isostatic response of the Australian lithosphere: Estimation of effective elastic thickness and anisotropy using multitaper spectral analysis. *Journal of Geophysical Research: Solid Earth,* v. 105(B8): 19163-19184.

Sinclair, H. D., B. J. Coakley, et al. (1991). Simulation of Foreland Basin Stratigraphy using a diffusion model of mountain belt uplift and erosion: An example from the central Alps, Switzerland. *Tectonics,* v. 10(3): 599-620.

Smith, C. C., J. F. Dahl, et al. (1996). The Duality of Leakage and Aliasing and Improved Digital Spectral Analysis Techniques. *Journal of Dynamic Systems, Measurement, and Control,* v. 118(4): 741-747.

Steckler, M. S. and U. S. t. Brink (1986). Lithospheric strength variations as a control on new plate boundaries: examples from the northern Red Sea region. *Earth and Planetary Science Letters,* v. 79(1): 120-132.

Stephenson, R. and K. Lambeck (1985a). Isostatic response of the lithosphere with in-plane stress: Application to central Australia. *Journal of Geophysical Research: Solid Earth,* v. 90(B10): 8581-8588.

Timoshenko, S. and S. Woinowsky-Krieger (1959). Theory of plates and shells. McGraw-Hill.

Turcotte, D. L., R. J. Willemann, et al. (1981). Role of membrane stresses in the support of planetary topography. *Journal of Geophysical Research: Solid Earth,* v. 86(B5): 3951-3959.

Van Schmus, W. R., M. E. Bickford, et al. (1993). Proterozoic Geology of the Western Midcontinent Basement. Precambrian Conterminous U.S. J. C. Reed et al. Boulder. *Geological Society of America*. v. C-2: 239–259.

Viele, G. W. and W. A. Thomas (1989). Tectonic synthesis of the Ouachita orogenic belt. The Appalachian-Ouachita Orogen in the United States. J. R. D. Hatcher et al. *Geological Society of America*. v. F-2.

Walcott, R. I. (1970a). Flexural rigidity, thickness, and viscosity of the lithosphere. *Journal of Geophysical Research,* v. 75(20): 3941-3954.

Walcott, R. I. (1970b). Flexure of the lithosphere at Hawaii *Tectonophysics,* v. 9(5): 435-446.

Walper, J. L. (1977). Paleozoic tectonics on the southern margin of North America. *Transactions of the Gulf Coast Association of Geologic Society,* v. 27: 230-241.

Watts, A. B. (1978). An analysis of isostasy in the world's oceans 1. Hawaiian-Emperor Seamount Chain. *Journal of Geophysical Research: Solid Earth,* v. 83(B12): 5989-6004.

Watts, A. B. (2001). Isostasy and Flexure of the Lithosphere. Cambridge. Cambridge University Press.

Watts, A. B., J. H. Bodine, et al. (1980). Observations of flexure and the state of stress in the oceanic lithosphere. *Journal of Geophysical Research: Solid Earth,* v. 85(B11): 6369-6376.

Watts, A. B. and E. B. Burov (2003). Lithospheric strength and its relationship to the elastic and seismogenic layer thickness. *Earth and Planetary Science Letters*, v. 213(1): 113-131.

Wickham, J., D. Roeder, et al. (1976). Plate tectonics models for the Ouachita foldbelt. *Geology*, v. 4(3): 173-176.

Windley, B. (1992). A Continent Revealed. The European Geotraverse. Cambridge University Press.

Wright, W. (2011). Pennsylvanian paleodepositional evolution of the greater Permian Basin, Texas and New Mexico: Depositional systems and hydrocarbon reservoir analysis. *AAPG Bulletin*, v. 95(9): 1525-1555.

Yang, K.-M. and S. Dorobek (1995a). The Permian Basin of West Texas and New Mexico: Tectonic history of a "composite" foreland basin and its effects of stratigraphic development. Stratigraphic Evolution of Foreland Basins. S. L. Dorobek and G. M. Ross. *SEPM Society for Sedimentary Geology*. v. 52: 149-174.

Yang, K. M. and S. Dorobek (1995b). The Permian Basin of West Texas and New Mexico: Flexural Modelling and Evidence for Lithospheric Heterogeneity across the Marathon Foreland. Stratigraphic Evolution of Foreland Basins. S. L. Dorobek and G. M. Ross. *SEPM Society for Sedimentary Geology*. v. 52: 37-50.

Ye, H., L. Royden, et al. (1996). Late Paleozoic deformation of interior North America: The greater Ancestral Rocky Mountains. *AAPG Bulletin*, v. 80(9): 1397-1432.

Zhong, S. (1997). Dynamics of crustal compensation and its influences on crustal isostasy. *J. Geophys. Res.*, v. 102(B7): 15287-15299.

Zuber, M. T., T. Bechtel, et al. (1989). Effective Elastic Thicknesses of the Lithosphere and Mechanisms of Isostatic Compensation in Australia. *J. Geophys. Res.*, v. 94(B7): 9353-9367.